Nucleic Acids Research, 2023, **51**, 11258–11276
https://doi.org/10.1093/nar/gkad774
Advance access publication date: 4 October 2023
RNA and RNA-protein complexes

Drosha-dependent microRNAs modulate FUS-mediated neurodegeneration *in vivo*

Sukhleen Kour[1], Tyler Fortuna[1], Eric N. Anderson[1], Darilang Mawrie[1], Jessica Bilstein[2], Ramakrishnan Sivasubramanian[2], Caroline Ward[1], Rishit Roy[1], Dhivyaa Rajasundaram[3], Jared Sterneckert[2,4] and Udai Bhan Pandey[1,5,*]

[1]Department of Pediatrics, Children's Hospital of Pittsburgh, University of Pittsburgh Medical Center, Pittsburgh, PA 15224, USA
[2]Center for Regenerative Therapies TU Dresden (CRTD), Technische Universität (TU) Dresden, Dresden, 01307, Germany
[3]Department of Pediatrics, Division of Health Informatics, Children's Hospital of Pittsburgh, Pittsburgh, PA 15224, USA
[4]Medical Faculty Carl Gustav Carus of TU Dresden, Dresden, 01307, Germany
[5]Children's Neuroscience Institute, Children's Hospital of Pittsburgh, University of Pittsburgh Medical Center, Pittsburgh, PA 15224, USA
[*]To whom correspondence should be addressed. Tel: +1 412 692 3192; Email: udai@pitt.edu

Abstract

Mutations in the Fused in Sarcoma (FUS) gene cause the familial and progressive form of amyotrophic lateral sclerosis (ALS). FUS is a nuclear RNA-binding protein involved in RNA processing and the biogenesis of a specific set of microRNAs. Here we report that Drosha and two previously uncharacterized Drosha-dependent miRNAs are strong modulators of FUS expression and prevent the cytoplasmic segregation of insoluble mutant FUS *in vivo*. We demonstrate that depletion of Drosha mitigates FUS-mediated degeneration, survival and motor defects in *Drosophila*. Mutant FUS strongly interacts with Drosha and causes its cytoplasmic mis-localization into the insoluble FUS inclusions. Reduction in Drosha levels increases the solubility of mutant FUS. Interestingly, we found two Drosha dependent microRNAs, miR-378i and miR-6832–5p, which differentially regulate the expression, solubility and cytoplasmic aggregation of mutant FUS in iPSC neurons and mammalian cells. More importantly, we report different modes of action of these miRNAs against mutant FUS. Whereas miR-378i may regulate mutant FUS inclusions by preventing G3BP-mediated stress granule formation, miR-6832–5p may affect FUS expression via other proteins or pathways. Overall, our research reveals a possible association between ALS-linked FUS mutations and the Drosha-dependent miRNA regulatory circuit, as well as a useful perspective on potential ALS treatment via microRNAs.

Graphical abstract

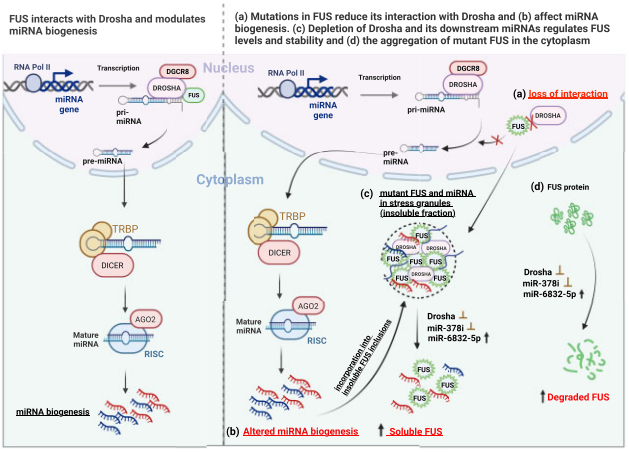

Introduction

RNA-binding proteins (RBPs) are evolutionary conserved effector molecules that are crucial for regulating spatial and temporal gene expression in the central nervous system (1–4). Various disease-causing mutations in RBP-encoded genes lead to disruption of RNA or protein stoichiometry, cause dysregulated nucleocytoplasmic shuttling, aggregation and defective RNA metabolism in a wide range of neurodegenerative and neurological diseases (5–7). Among them, amyotrophic lateral sclerosis (ALS), a lethal neuromuscular disorder characterized by progressive loss of nerve cells, muscle wasting and paralysis, is caused by autosomal dominant

Received: January 19, 2023. **Revised:** August 3, 2023. **Editorial Decision:** August 25, 2023. **Accepted:** September 12, 2023

mutations in various RBPs such as TDP-43, FUS, MATR3, TAF15, TIA1, hnRNPA2/B1 and hnRNPA1 (5,8–10). Around 90% of ALS cases are non-inherited and sporadic (sALS), whereas the rest (5–10%) are inherited (familial ALS) genetically >25 genes (11–13). FUS (Fused in Sarcoma, also known as Translocated in Liposarcoma) is one of several RBPs implicated in ALS, including the most aggressive, early-onset forms of ALS, along with structurally and functionally related TDP-43, MATR3 and hnRNP A1 (14–17). To date, >40 pathogenic mutations in FUS have been linked to ∼4% of the familial form of ALS. FUS is a ubiquitously expressed nuclear protein, and most of ALS-causing FUS mutations reside primarily in the C-terminal nuclear localization sequence, leading to impaired nuclear transport, nuclear depletion and toxic cytoplasmic aggregation of the mutant protein, which contribute to disease pathogenesis (14,18–21). Furthermore, the prognosis in a few ALS patients suggests that elevated physiological levels of wild-type (WT) FUS, in addition to the mutant protein's nuclear-cytoplasmic imbalance, may play a role in the pathogenesis of ALS (22,23).

FUS binds to RNAs through its conserved central RNA recognition motif, zinc finger motif and C-terminal arginine-glycine-glycine domain and regulates many aspects of DNA repair and RNA metabolism, including transcription (24), splicing (25), mRNA stability and transport (26,27), the biogenesis and processing of miRNAs (28–31). One plausible explanation for the FUS-mediated cellular toxicity observed in ALS could be the dysregulated mRNA processing due to nuclear–cytoplasmic imbalance and the uncontrolled accumulation of toxic mutant FUS in the cytoplasmic stress granules (32–35). Recent studies have shown that FUS interacts with non-coding RNAs to undergo RNA-mediated allosteric regulation, generating alternative protein interactions and transcriptional effects (36–38). Interestingly, FUS has been identified as one of the putative interactors of Drosha, a ribonuclease (RNase) III enzyme and indispensable component of the microprocessor complex required for instigating miRNA maturation in the nucleus by cleaving pri-miRNAs into precursor miRNAs (39–41). FUS controls the biogenesis of a subset of microRNAs by modulating Drosha activity and facilitating its binding to the transcriptional sites of pri-miRNAs (30). Furthermore, various miRNAs (miR141 and 200a) have been shown to regulate FUS gene expression, implying a complex interplay between FUS and microRNAs biogenesis (42). However, the direct role of Drosha and Drosha-dependent microRNAs in the regulation of mutant FUS activity in ALS has not been elucidated so far.

In this study, we described Drosha as an important regulator and genetic modifier of FUS- mediated toxicity. We found that depletion of Drosha significantly reduces FUS levels and mitigates eye degeneration and motor defects caused by mutant FUS expression in *Drosophila*. Surprisingly, the expression of mutant FUS caused the mislocalization of nuclear Drosha into cytoplasmic FUS puncta. We observed that abolishing Drosha levels and its activity strongly reduces FUS levels and prevents the incorporation of insoluble mutant FUS into cytoplasmic stress granules. More importantly, through microRNA profiling, we identified two Drosha-dependent microRNAs, miR-378i and miR6832-5p, which strongly modulate the levels and aggregation of insoluble mutant FUS in the cytoplasm. Interestingly, modulating miR-378i levels prevents G3BP-positive stress granule formation in the cytoplasm, suggesting that miR378i ameliorates mutant FUS inclusion into the stress granules by modulating G3BP-dependent stress granule dynamics. Overall, our results provide insight into the possible link between Drosha-dependent microRNAs and FUS-mediated ALS pathogenesis.

Materials and methods

Drosophila lines and assays

The FUS-WT, FUS-R518K, FUS-R521C and FUS-P525L lines were generated by site-specific insertion of the human transgene using the pUAST-attP2 vector at Best Gene Inc. UAS-RFP and FUS P525L-RFP lines have been described previously (43). The RNAi lines were purchased from the Vienna Drosophila Resource Center (VDRC). All stocks were cultured in a 12-hour light/dark cycle incubator on a standard dextrose medium.

Eye degeneration

Flies expressing wild-type and mutant FUS (R518K, R521C and P525L) in eyes under the control of an eye-specific driver, GMR-gal4, were crossed with Drosha deficiency and UAS-Drosha RNAi fly lines at 28°C. Adult female F1 progeny were separated, and their eye phenotype was captured using a Leica M205C microscope equipped with a Leica DFC450 camera. External eye degeneration was quantified using a previously published scoring system (44–46). Around 15–20 4-day-old progenies were objectively scored (2 points for 5% and 4 points for 50% affected area) based on abnormal bristle orientation, retinal collapse, ommatidial fusion, pitting and disorganization of the ommatidial array. Comparisons between genotypes were made using the Student's *t*-test.

Eclosion assay

UAS-FUS WT, R521C and R518K fly lines were crossed with motor neuron specific driver D42-gal4 in combination with a Drosha RNAi line at 28°C, and the eclosion of adult flies from puparia was monitored for 4 days. The percentage eclosed adult flies to the total number of puparia (eclosed and uneclosed) was calculated for each condition and normalized with controls.

Motor dysfunction assays

Larval crawling: third-instar larvae from the crosses between fly lines expressing UAS-Drosha RNAi and UAS-FUS WT and mutants (R521C and R518K) under the control of the motor neuron-specific driver, D42-gal4, were collected and their movements were measured in an agar petridish (47). The experiment was performed in triplicates with five larvae per replicate, and the distance crawled by each larva was recorded and measured per unit of time (velocity, cm/s) for each condition.

Rapid iterative negative geotaxis (RING) assay: UAS-FUS WT and mutant fly lines were crossed with either neuronal-specific inducible driver, ELAV Gene-switch ELAVGS-gal4, alone or in combination with Drosha RNAi, and day 1 female progenies were collected. The transgene was expressed by transferring the flies (10 flies per vial) to standard media mixed with 20 mM RU486 at 28°C, and locomotion was assessed by the RING assay after 9 days on drug food (47). Briefly, vials containing flies were tapped down against the bench, and the climbing was recorded on video for 45 seconds. The climbing ability of flies was assessed either by calculating

the distance climbed by each fly per unit time (velocity) or by measuring the percentage of flies reaching the 5 cm mark in 10 s. Quantifications were performed manually by a third party in a blinded manner, and data was normalized with *w1118* control flies.

Life span assay

One-day-old female F1 flies carrying UAS-FUS WT and mutant transgenes with or without Drosha RNAi were fed on fly food containing 20 mM RU486 (20 flies per vial, total flies = 100). RU486 mediates the expression of transgenes in fly neurons by the inducible ELAVGS-gal4 system. The number of dead flies was recorded every alternate day, and the percentage survival was calculated by the Kaplan–Meier survival plot. *w1118* flies crossed with ELAVGS-gal4 alone were used as controls.

Immunohistochemistry (IHC)

Brains of third-instar larvae expressing either P525L-RFP alone or in combination with Drosha RNAi were fixed in 4% paraformaldehyde and processed as described previously (48). The brains were incubated with mouse anti-lamin Dmo antibody (DSHB, 1:200) overnight, washed and probed with anti-mouse Alexa Flour 647 (Invitrogen # 28181, 1:100). The brains were mounted using DAPI-Fluoroshield (SIGMA, #F6182), and images were taken using a Nikon A1 Eclipse Ti confocal microscope. For quantification, five different confocal images from four different fly brains were used to calculate the number of cells with cytoplasmic FUS puncta. Student's *t*-test was used to calculate the *P* value between the two groups.

Mammalian cell culture and transfections

Human embryonic kidney 293T (HEK293T) (ATCC® CRL-3216™) and N2a cells were cultured in Advanced Dulbecco's Modified Eagle Medium supplemented with 10% FBS and 1% Glutamax at 37°C and 5% CO_2. Drosha knockout (DKO) HEK293 cells were a gift from Dr Shuo Gu (49). FUS induced pluripotent stem cells (iPSCs) are well-established CRISPR/Cas9-edited lines with isogenic controls used in various published works (50,51). iPSCs were cultured on Matrigel-coated plates in mTeSRTM-1 media (STEMCELL Technologies).

HEK293T cells were transiently transfected with plasmid constructs for 24–48 hours by using Turbofect (Invitrogen). miRNA transfections were performed for 48 hours using Lipofectamine™ RNAiMAX transfection reagent (Thermo Fisher). Doxycycline-inducible and stable FUS WT, FUS R521C and FUS P525L N2a lines (52) were induced with 400 ng/ml of doxycycline for 48 hours after the transfections.

Plasmids

HA-tagged FUS WT, FUS-R518K and FUS-R521C cDNA constructs were previously generated in our laboratory (45). HA-tagged FUS WT and FUS-R521C cDNA constructs with 3′ untranslated region (UTR) were custom designed by Vector builder. The GFP-Drosha WT construct was a gift from Dr. Shuo Gu (49). S300A/S302A Drosha and myc-Drosha were purchased from Addgene.

Differentiation of iPSCs into neuronal cells

FUS iPSCs were differentiated into neurons by following the previously described protocol (53). Briefly, 80–90% confluent and well-spread iPSCs were grown for 7 days in Neurobasal/Dulbecco's Modified Eagle Medium-F12 medium (1:1 v/v) containing 2% B27 (Gibco, 17054–044), 1% N2 (Gibco, 17502–048), 1% Glutamax (Gibco) and 1% non-essential amino acids (Gibco, 11140050) along with SB431542 (STEMCELL Tpechnologies), LDN (Sigma SML0559), smoothened agonist (Cayman Chemicals 11914) and retinoic acid (Sigma R2625). For the the next 5 days, cells were grown in neurobasal-N2-B27 media supplemented with retinoic acid, smoothened agonist, DAPT (N-[2S-(3,5-difluorophenyl)acetyl]-L-alanyl-2-phenyl-1,1-dimethylethyl ester-glycine) (Cayman, 13197) and SU5406 (Cayman, 131825). On day 14, cells were dissociated and cultured on poly-ornithine and laminin-coated plates in neurobasal-N2-B27 media containing growth factors (BDNF, GDNF, CNTF) and ascorbic acid (Sigma, A4403). The differentiated neurons were processed for subsequent immunofluorescence and western blot analyses after 28 days.

Immunofluorescence (IF)

For IF, cells were processed as previously described (53). Briefly, cells were fixed in 4% paraformaldehyde and blocked in 5% normal goat serum for 15 min. The cells were incubated overnight at 4°C with the primary antibodies: mouse anti-Drosha (Santa Cruz, 1:200), mouse anti-HA (Sigma, 1:1000), rabbit anti-HA (Invitrogen, 1:1000) and anti-rabbit G3BP (Thermo Fisher, 1:1000). The following day, cells were washed thrice with PBS-1% TritonX-100 and incubated with secondary antibodies: Alexa Fluor-488, Alexa Fluor-568 and Alexa Fluor-647 (Invitrogen, 1:1000) for 2 hours. The cells were washed with PBS-1% TritonX-100 and mounted using Fluoroshield™ containing DAPI (Sigma). All the images were taken on Nikon A1 eclipse Ti confocal microscope.

The percentage of cells with FUS puncta was quantified from 7–8 different x60 confocal images from three different coverslips, with each image containing 14–20 cells in total. For Drosha S300A/S302A expression analysis, cells cotransfected with FUS (WT and mutants) and cytoplasmic S300A/S302A from 6–8 confocal images were used. Student's *t*-test was used to calculate the significance (*P* value) between the two groups.

Western blotting (WB)

The cells were lysed in RIPA-lysis buffer: 150 mM NaCl, 50 mM NaF, 2 mM EDTA, 0.2 mM sodium orthovanadate, 1% sodium deoxycholate, 2 mM DTT, 1% NP40, 0.1% SDS and protease inhibitor (Roche 11836170001). After determining the concentration with the Pierce™ BCA protein assay kit (Thermo Scientific 23227), around 40 μg of protein was separated using either 4–12 Bis-Tris or 3–8% Tris-acetate NuPage gel (Novex/Life Technologies). The proteins were transferred onto nitrocellulose membranes (Invitrogen IB23001), incubated in 2.5% QuickBlocker reagent (EMB Millipore WB57-175GM) for 1 hour at room temperature and probed overnight at 4°C with primary antibodies. The blots were incubated with secondary antibodies for 1 hour, washed with 1% Tween-20 in Tris buffered saline and imaged.

For quantification, each protein lysate from three different transfections (biological replicates) was run in duplicates or triplicates (2–3 technical replicates). Anti-FUS antibody used in the study (Bethyl and Thermo Fisher) probed for both post-transcriptionally modified (upper band) and unmodified (lower band) FUS protein. IDV values from the upper FUS

band were measured using Fiji/Image Studio, normalized with either Tubulin or GAPDH, and plotted in a scatter bar graph. A one-way analysis of variance (ANOVA) with a Bonferroni *post hoc* multiple comparison test was used to calculate the significance (*P*) between the three groups.

Co-immunoprecipitation

Lysates were prepared from HEK cells co-transfected with GFP-DROSHA and HA-tagged FUS WT or mutants (R5218K and R521C) in buffer containing 10 mM Tris–HCl (pH 7.5), 100 mM NaCl, 2.5 mM $MgCl_2$, 2 mM DTT, 2.5 mM sodium orthovanadate, 0.1% NP40 and 1x protease inhibitor cocktail (Invitrogen). The lysates (400 μl) were incubated with either rabbit anti-HA (Invitrogen) or mouse anti-GFP (Santa Cruz) antibodies overnight at 4°C. The antibody-protein complex was incubated with 80 μl of Protein G superparamagnetic beads (Invitrogen 10004D) for 4 h at 4°C, followed by subsequent washes and precipitation using MagnaRack™ (Invitrogen CS15000). The RNA-dependent interaction between FUS and Drosha was assessed by treating the cell extracts with 1 mg/ml RNase A for 1 hour at 4°C before starting the immunoprecipitation with mouse GFP antibody. The immunoprecipitated samples were resuspended in 1x NuPage™ LDS-Sample buffer (Invitrogen NP0007), followed by SDS–PAGE and immunoblotting.

For quantification, three independent immunoprecipitation blots ($n = 3$) were analyzed and the calculated IDV values of precipitated HA-FUS were normalized to Drosha-GFP. A scatter bar graph was plotted, and Student's *t*-test was used to determine the significance.

Soluble–insoluble protein fractionation

For soluble–insoluble fractionation, HEK293T cells and differentiated FUS neurons transfected with miR-6832–5p mimic or antagomir-378i were resuspended in NP40 lysis buffer: 0.5% NP40, 10 mM Tris HCl pH 7.8, 10 mM EDTA, 150 mM NaCl, 2.5 mM Na orthovanadate, 1x protease inhibitor cocktail (Roche 11836170001). The cell extracts were sonicated and centrifuged at 21 000*g* for 30 min. The supernatant (soluble fraction) was collected, and the pellet was resuspended in re-solubilization buffer: 50 mM Tris HCl pH 6.8, 5% SDS, 10% glycerol, followed by sonication and centrifugation at 12 000*g* for 10 min (insoluble fraction). The soluble and insoluble fractions were boiled in 1x NuPage™ LDS-Sample buffer at 95°C for 5 min, separated by SDS–PAGE, and immunoblotted. Three independent immunoblots were quantified ($n = 3$), and significance was measured using the Student's *t*-test.

Stability assay

To assess the effect of Drosha on the degradation of endogenous or HA-tagged FUS, HEK293T and DKO cells were transfected with HA-FUSWT and HA-R521C plasmids for 24 hours. The cells were harvested and lysed in RIPA-lysis buffer after 0, 3, 6, 12, 24 and 36 hours of 100 μg/ml cycloheximide (CHX) treatment. The total protein extract was resolved by SDS–PAGE, followed by immunoblotting, as indicated above. IDVs were normalized to GAPDH based on three independent gels. A linear regression graph was plotted, and a half-life estimate of FUS protein in HEK293T and DKO cells was calculated.

All the antibodies were prepared with 2.5% QuickBlocker reagent. The blots were imaged using Odyssey® CLx (LI-COR Biosciences). All samples were run in triplicates and the integrated band densities (IDVs) were calculated in the image studio software (LI-COR).

Primary antibodies used were: mouse anti-tubulin (SIGMA, 1:10 000), mouse anti-Drosha (Santa Cruz, 1:200), mouse anti-HA (Sigma, 1:2000), rabbit anti-HA (Invitrogen, 1:5000) and rabbit anti-FUS (Bethyl, 1:2000).

Secondary antibodies used were: anti-rabbit DYLight 800 and anti-mouse 680 (Invitrogen, 1:10 000).

Quantitative OCR

RNA was isolated from cells and neurons by using the PureLinkTM RNA mini kit (Invitrogen), following the manufacturer's instructions. RNA concentration and purity (260/280 and 260/230 ratios) were determined using a NanoDrop ND-1000 spectrophotometer. Around 300 ng of total RNA was reverse transcribed to cDNA by using iScript™ Reverse Transcription Kit (BioRad). Quantitative PCR was performed on 1/10th of the cDNA using a custom-designed 5′ 6-FAM/ZEN/3′ IBFQ IDT PrimeTime Assay Set (Supplementary Table 1) in a 7300 real-time PCR machine (Applied Biosystems). Using GAPDH as an internal control, gene expression (C_t values) was normalized across 4–5 replicates.

In flies, RNA was isolated using TRizol (Ambion; 15596026) as previously described (17,43,45,46). Around nine fly heads were used for RNA extraction, and gene expression was normalized with tubulin.

Small RNA profiling

For small RNA sequencing, HEK293T and CRISPR/Cas9-edited DKO cells were transfected with FUS WT and FUS R521C plasmid constructs without 3′ UTR for 24 hours. Small RNAs (<200 nt) were isolated using mirVana™ miRNA Isolation Kit (Invitrogen), and profiling was performed on 1 μg of total RNA using BGI's DNBSEQ™ small RNA sequencing platform. For quality control, 18–30 nt RNA segments were separated by PAGE gel, followed by adaptor ligation and real-time PCR amplification of cDNAs. All the contaminant adaptors or tags were removed, and the length distribution of clean reads (between 18 and 30 nt) was summarized. Reads were mapped to the human reference genome and to other sRNA databases using Bowtie2 (54), and gene expression levels were calculated using Transcripts Per Kilobase Million (TPM). Differentially expressed small RNAs were screened by DESeq2 based on the negative binomial distribution (55), and the significance of gene expression differences was calculated using an adjusted $P \leq 0.1$ and the absolute value of $\log_2$ratio ≥ 1. Hierarchical clustering of differentially expressed miRNA was performed using pheatmap function, and several software programs such as RNAhybrid, miRanda or TargetScan were used to predict the small RNA targets (56–58).

miRNA real time PCR

For miRNA quantification and validation, HEK293T and DKO cells were transfected with FUSWT, R518K and R521C for 24 hours with Turbofect (Invitrogen), and total RNA was isolated using MagMAX™ mirVana™ Total RNA Isolation Kit (Applied Biosystems™) by following the manufacturer's instructions. 30 ng of RNA were reverse transcribed by using the TaqMan™ MicroRNA Reverse Transcription Kit (Applied

Biosystems™) and miRNA-specific primers (Supplementary Table S1), followed by real-time PCR using TaqMan™ Universal Master Mix II with UNG (TaqMan assays, Applied Biosystems™). Using U6snRNA as internal control, the C_t values were normalized across 4–5 replicates.

The soluble and insoluble fractionation of mRNA was performed by following the previously published protocol with some modifications (59). Briefly, DOX induced FUS WT, R521C and P525L N2a cells were treated with 0.25 mM sodium arsenite for 1 h and collected by centrifugation at 4000*g* for 5 min. Cells were resuspended with PBS and subjected to three cycles of freeze-thawing. The cell extract was centrifuged at 17 800*g* for 10 minutes at 4°C. RNA from supernatants and precipitates containing the soluble and insoluble fractions, respectively, was isolated was isolated using MagMAX™ mirVana™ Total RNA Isolation Kit (Applied Biosystems™) and analyzed by real-time PCR.

miRNA transfections and assays

miRNA antagomirs and mimic with 2′-O-methyl residues and ZEN modifications were custom generated and purchased from IDT. HEK293T, DOX-inducible FUS-N2a cells, and differentiated neuronal cells were transfected with 100 nM of miRNA antagomirs and mimic for 48 hours by using Lipofectamine™ RNAiMAX (Invitrogen) and processed for subsequent real-time PCR and immunoblotting (described previously). FUS was induced in stable FUS WT, R521C and P525L-N2a cells by 400 ng/ml of Doxycycline (DOX) for 48 hours along with miRNA transfection.

Statistical analysis

All the statistical analyses were performed on GraphPad Prism v.8 software. Comparisons between two groups were performed by Student's *t*-test. A one-way ANOVA with Bonferroni or Tukey *post hoc* multiple comparison tests was applied for more than two comparisons.

Results

Depletion of Drosha affects FUS expression and phenotypes *in vivo*

Previously, through an unbiased genome-wide screen in *Drosophila* (45), we identified Drosha as one of the genetic modulators of mutant FUS-mediated toxicity. Drosha is a part of the microprocessor complex, and FUS is required for miRNA-mediated gene silencing through its interaction with Drosha (29,39). To further validate whether Drosha acts as a potential modifier of FUS-associated ALS, we utilized the well-established *Drosophila* FUS-ALS model system (45,51,60) for examining the various attributes of ALS-mediated manifestations such as eye degeneration, motor dysfunction and reduced life span (Figure 1). By using the GAL4/upstream activation sequence (UAS) system and an eye-specific promoter (GMR), we expressed human FUS WT and ALS-linked FUS mutants (R521C and R518K) in *Drosophila* eyes with or without Drosha- specific RNAi (Figure 1a). We found that reducing the levels of Drosha, as validated by qPCR (Figure 1c), significantly alleviated eye degeneration in FUS-expressing flies as compared to EGFP controls (Figure 1a and b). Importantly, FUS WT and mutant flies expressed significantly higher levels of Drosha mRNA as compared to EGFP controls (Supplementary Figure S1a). Using RNAi-mediated knockdown of Drosha, we observed a significant reduction in FUS protein levels in fly neurons, suggesting that Drosha-mediated suppression could be due to a reduction in the levels of toxic FUS protein (Figure 1d and e).

As ALS predominantly affects the motor neurons (61), we asked whether RNAi-mediated loss of Drosha could influence the motor function defects in FUS expressing fly neurons. We expressed Drosha RNAi in motor neurons of WT and mutant FUS flies by using the motor neuron-specific driver D42-GAL4 and examined the crawling ability of third-instar larvae and their eclosion into adults. We found strong eclosion defects, as measured by the percent of adult flies to the total number of puparia, in wild-type and mutant FUS flies, which are significantly restored by reduced Drosha levels (Figure 1f). Similarly, we noticed a significant improvement in the locomotor ability of larvae, as determined by total distance traveled per unit time (velocity), in FUS flies expressing Drosha RNAi (Figure 1g). To further assess any motor-related behavioral changes, we conducted a rapid iterative negative geotaxis (RING) assay in adult flies expressing the FUS transgene in combination with Drosha RNAi in fly neurons by using an inducible ELAVGS-GAL4 promoter. We found that loss of Drosha significantly ameliorated the climbing ability of FUS-expressing flies, as determined by calculating either the percentage of flies that can climb above 5 cm in 10 s (Figure 1h) or the distance climbed by a fly per second (Figure 1i), respectively. As ALS is a fatal condition with an average life expectancy of 2–5 years after diagnosis, we investigated the effect of loss of Drosha on the life span of flies expressing WT and R521C in fly neurons. We found that depletion of Drosha increased the survivability of FUS WT and R521C flies as compared to FUS-alone controls (Figure 1j–l, and Supplementary Figure S1b). While R518K-expressing flies showed a moderate change in overall survivability by Drosha RNAi, we found that Drosha depletion notably increased the number of days to reach 50 and 75% mortality as compared to R518K-alone flies (Supplementary Figure S1b). Overall, we discovered that Drosha is a genetic modifier of FUS toxicity *in vivo* and that lowering its levels reduces FUS-mediated neuronal defects and lethality by lowering toxic FUS protein levels.

FUS mutations regulate Drosha levels and localization pattern in iPSC neurons and mammalian cells

We assessed the expression of Drosha in patient-derived FUS-R521C lymphoblastoid cells by qPCR and found a significant upregulation in Drosha RNA levels as compared to age-matched controls (Figure 2a). As FUS is a known interactor of Drosha (39), we investigated whether ALS causing FUS mutations affect its interaction with Drosha. We performed co-immunoprecipitation to pull down the GFP-Drosha by using anti-HA antibodies and vice versa from the HEK293T cell lysates co-transfected with GFP-Drosha and HA-tagged FUS WT, R518K and R521C, respectively (Figure 2b). We found a strong and increased interaction of Drosha with FUS-R521C compared to FUS WT (Figure 2c). To further determine whether Drosha and FUS interaction requires RNA, we immunoprecipitated HA-FUS with anti-GFP antibody in the presence or absence of 1mg/ml RNase in HEK293T cells co-transfected with FUS (WT, R518K and R521C) and Drosha-GFP (Figure 2d). We found that levels of HA-FUS immunoprecipitates were significantly decreased in

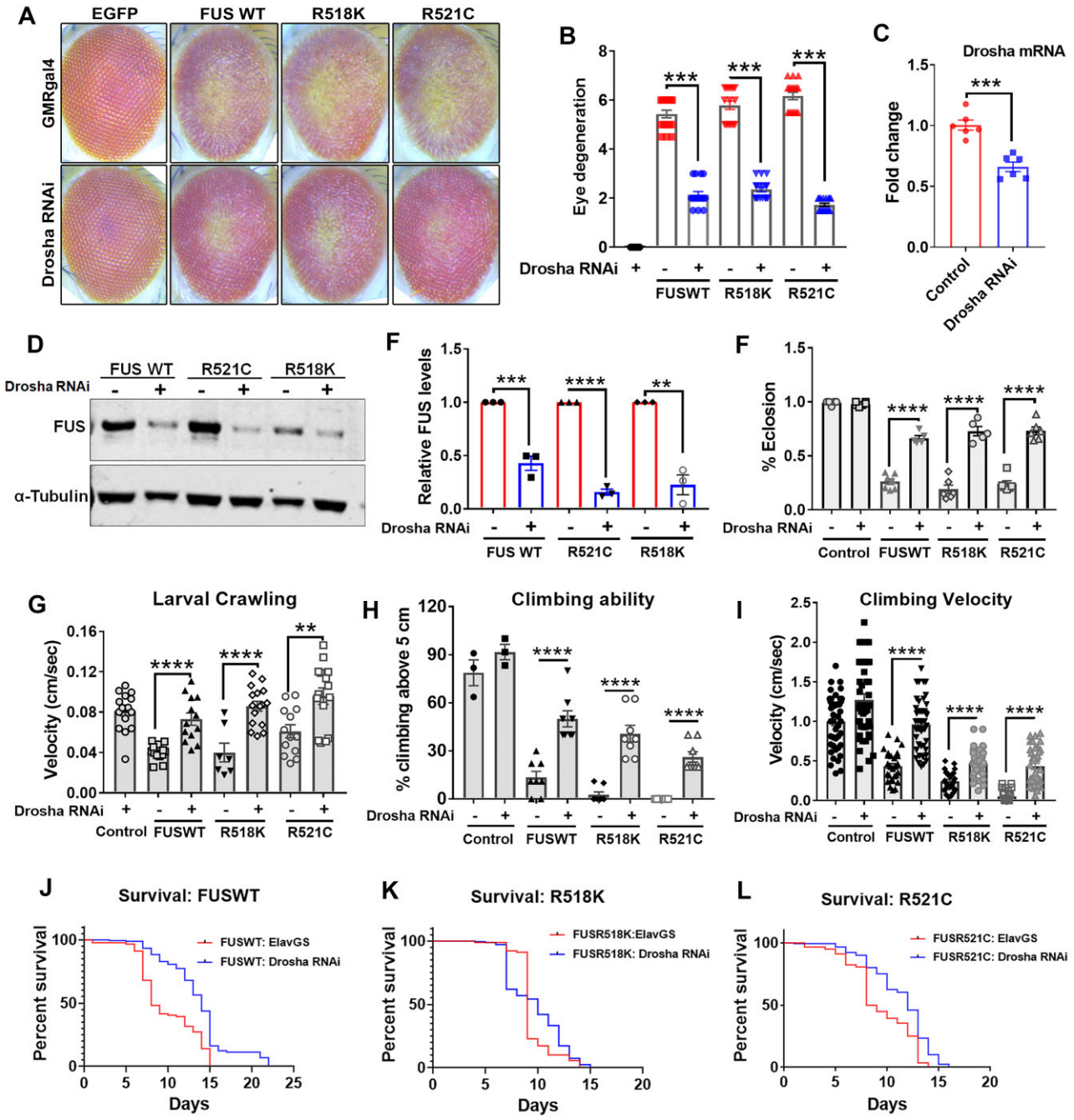

Figure 1. Drosha is a genetic modifier of FUS-mediated toxicity *in vivo*. (**A**) Representative eye images of flies expressing wild-type and mutant FUS (R518K, R521C) when crossed with EGFP control and Drosha RNAi flies (**B**) Bar graph showing that in the absence of Drosha, the severity of eye degeneration as shown in (**A**) was significantly reduced in FUS wild-type and mutants ($n = 18$). (**C**) qPCR showing the significant reduction of Drosha mRNA in the Drosha-RNAi fly line. Tubulin mRNA was used as a normalization control (two-tailed unpaired *t*-test, $n = 3$). (**D**) Representative immunoblot showing FUS levels in fly neurons expressing WT and mutant FUS in the presence and absence of Drosha RNAi. (**E**) Quantitative bar graph in (**D**) showing the significant decrease in FUS protein levels in wild-type and mutant FUS (R518K and R521C) fly neurons upon knockdown of Drosha. Tubulin was used as a normalization control (two-tailed unpaired *t*-test, $n = 5$). (**F**) Bar graph depicting the eclosion defect in flies expressing WT and mutant FUS, as measured by the percentage of eclosed adults relative to the total number of pupae, and its rescue by RNAi-mediated Drosha knockdown (two-tailed unpaired *t*-test, n = 4–7). (**G**) Bar graph showing that the crawling defect (measured as distance traveled in 1 minute) was significantly rescued by the RNAi-mediated KD of Drosha in third-instar larvae expressing WT and mutant FUS under the control of motor neuron driver, D42-gal4. UAS-Drosha RNAi lines crossed with a motor neuron-specific driver (D42-gal4) were used as comparative controls (two-tailed unpaired *t*-test, $n = 27$–52). (**H**, **I**) Bar graph representing RING assay, calculated as climbing speed of a fly per second (**H**) and the percentage of flies climbing above 5 cm in 10 s (**I**), showed significant improvement in the climbing abilities of flies expressing wild-type and mutant FUS on Drosha knockdown. W1118 and UAS-Drosha RNAi flies crossed with ELAVGS-gal4 driver lines were used as comparative controls (two-tailed Mann–Whitney *U*-test). (**J**–**L**) Kaplan–Meier survival plots showing the effect of loss of endogenous Drosha on the life span of flies expressing WT (**J**) and mutant FUS, R518K (**K**) and R521C (**L**) transgenes under the inducible neuronal ELAV-UAS gal4 system, respectively. One-day-old female flies expressing the transgene were grown on 20 mM RU486 drug food to express the transgene and monitored every day for the span of 40 days (log-rank (Mantel–Cox) test, $n = 80$). The data represent mean ± SEM. *P* values (****<0.0001, ***<0.001, **<0.01).

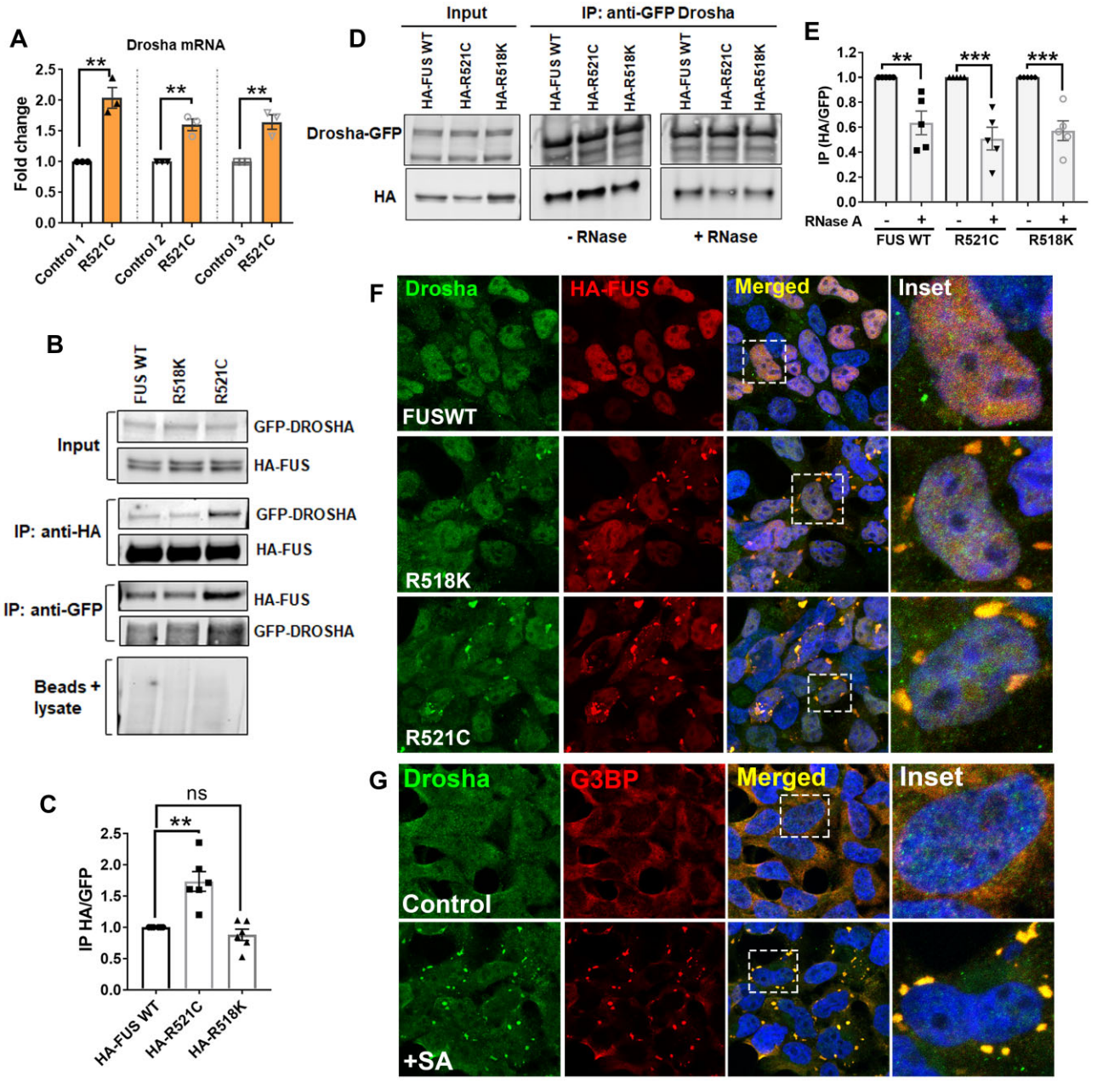

Figure 2. Mutant FUS elevates endogenous Drosha levels and promotes its sequestration in the cytoplasmic stress granules. (**A**) Bar plot showing Drosha mRNA levels in patient lymphoblastoid cells carrying FUS R521C mutation as compared to three age-matched controls. GAPDH was used as a normalization control (two-tailed unpaired *t*-test, $n = 3$). (**B**) Co-immunoprecipitation blots showing the interaction between FUS and DROSHA in HEK293T cells co-transfected with GFP-tagged Drosha and HA-tagged FUS (WT, R518K and R521C) for 24 h. Anti-GFP and anti-HA antibodies were used to precipitate HA-FUS and Drosha-GFP, respectively. Beads incubated with protein extract were used as a negative control. (**C**) Scatter bar plot showing an increased interaction of HA-FUS R521C with Drosha-GFP as compared to FUS WT and R518K as shown in (**B**). The graph represented the levels of precipitated HA-FUS relative to Drosha GFP across five replicates ($n = 5$, one-way ANOVA) (**D**) Representative blots depicting the immunoprecipitation of HA-FUS by Drosha-GFP in the presence or absence of 1 mg/ml RNase A in HEK293T cells transfected with HA-FUS WT and mutants. (**E**) Bar graph showing the levels of precipitated HA-FUS by Drosha-GFP. The interaction of FUS and Drosha showed a significant decrease in RNase A treated lysates as compared to untreated groups ($n = 5$, two-tailed unpaired *t*-test). The data (1a, 1c, and 1e) represent mean ± SEM. *P* values ***<0.001, **<0.01). (**F**) IF images showing the colocalization of endogenous Drosha with FUS in HEK293T cells transfected with HA-FUSWT, HA-R518K and HA-R521C. Inset images show the sequestration of nuclear DROSHA into cytoplasmic FUS puncta in R518K and R521C expressing cells versus FUSWT. (**G**) IF images of HEK293T cells treated with 0.25 mM sodium arsenite for 1 hour showed localization of endogenous nuclear Drosha into cytoplasmic G3BP-positive stress granules as compared to untreated cells. All microscopic images were taken at x60 optical magnification, and DAPI was used to mark the nucleus.

RNase-treated lysates compared to untreated controls, suggesting an RNA-dependent interaction between Drosha and FUS (Figure 2e).

FUS is predominantly nuclear, and ALS-linked mutations in FUS lead to its mislocalization and irreversible segregation into the cytoplasmic inclusions and stress granules (33,62). As these FUS inclusions have been shown to exert pathogenicity through toxic gain of function by sequestration of various other RNAs and proteins (63,64), we asked whether ALS-linked FUS mutations (R518K and R521C) modulate the expression and localization of endogenous Drosha. We overexpressed HA-tagged FUS WT, R518K and R521C in HEK293T cells to determine their impact on the subcellular localization of endogenous Drosha. Drosha is a part of nuclear complex protein and we found that mutant R518K, and R521C sequestered Drosha into cytoplasmic FUS inclusions as compared to the FUS WT, indicating that mutant FUS could possibly influence Drosha function by promoting its mislocalization and increased expression (Figure 2a and f). The aggregation of mutant FUS in the cytoplasmic stress granules (SGs) is one of the pathological hallmarks of ALS. By IF, we analyzed the sub-cellular distribution of endogenous Drosha in HEK293T cells under stress conditions and found that the treatment with 0.25 mM sodium arsenite caused the entrapment of nuclear Drosha in the G3BP-positive cytoplasmic stress granules (Figure 2g), mimicking the effect caused by pathological FUS mutants (Figure 2b). All these observations suggest that pathological FUS mutations may regulate Drosha expression and affect its cellular localization.

Knocking down Drosha prevents cytoplasmic FUS aggregation in mammalian cells and *in vivo*

The cytoplasmic amassing of mutant FUS protein in ALS has been associated with cellular toxicity and neuronal death (65,66). Since we established that the pathological mutations in FUS lead to increased Drosha expression and its sequestration in the cytoplasmic FUS puncta, we performed an analogous experiment in CRISPER/Cas9-edited DKO HEK293T cells to investigate if the loss of Drosha alleviates the agglomeration of mutant FUS puncta into SGs. We transfected HEK293T and DKO cells with HA-tagged wild-type and mutant FUS (R518K and R521C) for 24 hours and assessed the distribution of FUS puncta in G3BP- positive cytoplasmic stress granules (Figure 3a). We observed a profound mislocalization and accumulation of mutant FUS (R518K and R521C) in the cytoplasmic G3BP positive inclusions in HEK cells. In comparison, the percentage of cells with colocalized mutant FUS and G3BP positive puncta showed a significant reduction in DKO cells. On the other hand, FUS WT showed nuclear expression and no comparable change in distribution in control and DKO cells (Figure 3b). In a similar study, we found that ectopic expression of Drosha in DKO cells reinstated the cytoplasmic mislocalization and aggregation of mutant FUS (Supplementary Figure S2), suggesting that Drosha is crucial to prevent mutant FUS segregation in the cytoplasm. Since our *in vivo* data (Figure 1d and e) suggested a notable decrease in FUS protein levels upon Drosha knockdown, we recapitulated the findings and assessed the FUS levels by immunoblotting in DKO cells transfected with wild-type and mutant FUS (R518K and R521C) cDNA constructs. We found that loss of Drosha significantly decreased the endogenous (∼30–40%, Figure 3d) and ectopic (∼60–80%, Figure 3e) FUS protein levels as compared to controls (Figure 3c–e), indicating that reduced sequestration of mutant FUS into the cytoplasmic SGs on DKO could be due to a decrease in the overall levels of FUS protein. Since the FUS cDNA constructs used in this study lacked 3′UTR, we looked at how Drosha depletion affects the FUS expression in DKO or HEK293T cells transfected with FUS (WT and R521C) constructs with 3′UTR (Supplementary Figure S3a). Interestingly, analogous to our findings in Figure 3d, the DKO cells displayed significantly lower endogenous (∼40%) and HA-FUS (∼50%) protein levels compared to HEK293T cells (Supplementary Figure S3b and c), suggesting that Drosha could potentially function independent of 3′UTR to modulate FUS expression. Moreover, we found that Drosha depletion significantly reduced FUS mRNA levels in untransfected (Supplementary Figure S3d) and FUS (WT and mutants) transfected DKO cells (Supplementary Figure S3e). Furthermore, we supplemented our findings by examining the impact of Drosha depletion on the distribution and mislocalization of FUS puncta in fly motor neurons (Figure 3f and Supplementary Figure S4). We expressed the RFP-tagged mutant FUS-P525L transgene with or without Drosha RNAi in fly neurons by using the motor neuron-specific promoter OK-gal4 and evaluated the subcellular localization of FUS in the ventral nerve cord (VNC) region of the third instar larval brain by immunofluorescence (Figure 3f). We found an apparent mislocalization of mutant FUS to the cytoplasm of larval neurons expressing the FUS-P525L transgene and, on RNAi-mediated knockdown of Drosha, the number of cells with cytoplasmic P525L puncta showed a significant reduction *in vivo* (Figure 3g). On the other hand, no notable difference was observed in the nuclear localization of FUS WT protein in fly brains with or without Drosha RNAi (Supplementary Figure S4). Consequently, to better understand the indirect mechanism by which Drosha is responsible for the decreased FUS levels, we compared the stability of endogenous (Figure 3h) as well as ectopically expressed FUS WT (Figure 3j) and R521C (Figure 3l) in DKO and HEK293T cells. The rate of degradation of FUS protein analyzed after 0, 3, 6, 12, 24 and 36 hours of CHX treatment showed that ectopic FUS WT (Figure 3k) and R521C (Figure 3m) proteins were significantly unstable in Drosha KO (FUS WT $t_{1/2} = 23.9$ and R521C $t_{1/2} = 21.8$ hours, respectively) cells compared to HEK293T ($t_{1/2} = 44$ h) cells. On the other hand, endogenous FUS demonstrated a comparable, but slightly lower, rate of degradation ($t_{1/2} = 32.9$ h) by Drosha depletion compared to controls (Figure 3h and i), suggesting that in the absence of 3′UTR, FUS WT and R521C showed robust rate of degradation in DKO cells compared to controls. All in all, these findings indicate that the loss of Drosha not only affects the expression and stability of FUS, but also reduces the accumulation of mutant FUS in cytoplasmic stress granules.

Phosphorylation of Drosha is essential for regulating FUS toxicity

Drosha is a core component of the microprocessor complex, which instigates miRNA maturation in the nucleus by cleaving pri-miRNAs into precursor miRNAs (40,67). Drosha activity, subcellular localization and interaction with other co-factors and pri-miRNA are all known to be regulated by its phosphorylation at Serine 300 and 302 in the Arg/Ser rich N terminus region (68). To test the functional consequences of Drosha activity on ALS-linked mutant FUS

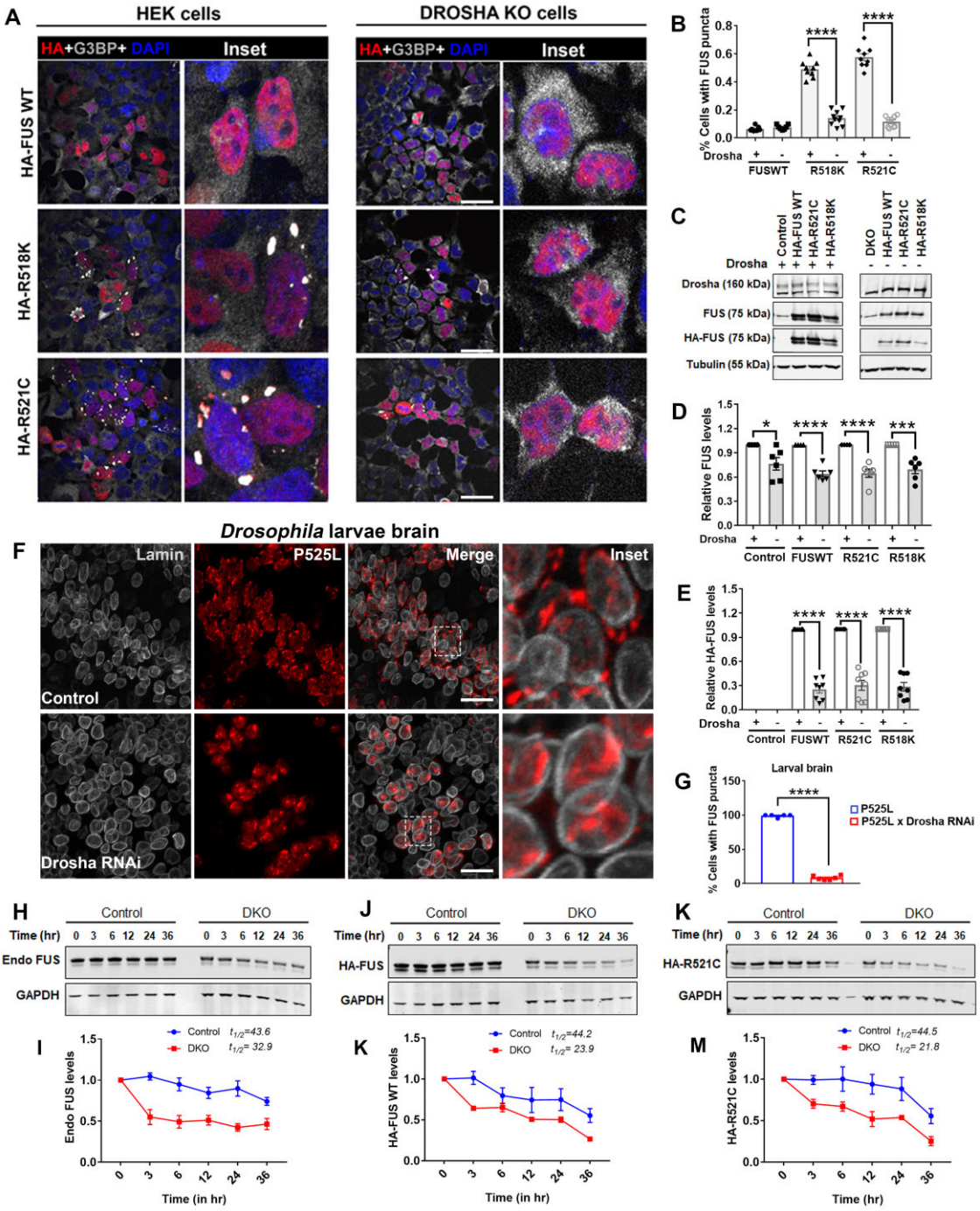

Figure 3. Abolishing endogenous DROSHA prevents mutant FUS aggregation: (**A**) Representative IF images of HEK293T and CRISPR/Cas9-edited DKO cells transfected with HA-FUSWT, HA-R518K and HA-R521C, respectively. Inset images showing a strong reduction in the cytoplasmic sequestration of mutant FUS in DKO cells (right two columns) as compared to controls (left two columns). All microscopic images were taken at x60 optical magnification, and DAPI was used to mark the nucleus. (**B**) Quantitative bar plot indicating a significant reduction in the percentage of cells with FUS puncta in DKO cells compared to controls, as shown in (**A**). For the quantification, seven to ten IF images with 14–20 cells each were used ($n = 7$–10, two-tailed unpaired *t*-test). (**C**) Representative immunoblots showing DROSHA, HA-FUS and endogenous FUS levels in HEK293T and DKO cells transfected with FUS WT, R518K and R521C cDNA constructs as compared to controls. Tubulin was used as a normalization control. (**D**, **E**) Bar graphs showing significant reduction in the levels of endogenous FUS (**D**) and HA-FUS (**E**) in DKO cells compared to controls ($n = 6$–8, two-tailed unpaired t test). (**F**) Representative IF images of third instar larval brain expressing the RFP-P525L transgene with or without Drosha RNAi under the control of motor neuron driver OK371-gal4. Inset images showing a significant reduction of cytoplasmic P525L puncta on RNAi mediated knockdown of Drosha. (**G**) Bar plot showing the significant decrease in the percentage of cells with cytoplasmic FUS puncta in P525L larval brain expressing Drosha RNAi as compared to controls. Five different confocal images from four different fly brain sections were used to calculate the number of cells with FUS puncta relative to total number of cells ($n = 5$ two-tailed unpaired *t*-test). (**H**–**M**) Representative blots showing the degradation of endogenous FUS (**H**) as well as transfected HA-FUS WT (**J**) and HA-R521C (**K**) in DKO and HEK293T cells after 0, 3, 6, 12, 24 and 36 hours of CHX treatment. Quantitative analysis on three independent blots showed an increased rate of depletion of endogenous FUS (**I**) as well as overexpressed HA-FUS WT (**K**) and HA-R521C (**M**) in DKO cells as compared to control. GAPDH was used as a normalization control ($n = 3$). The data (B, D, E, G, I, K and M) represent mean ± SEM. *P* values ****<0.0001, ***<0.001, *≤0.05).

toxicity, we co-transfected HEK293T cells with phospho-dead Drosha (Serine to Alanine change at 300/302 residue) and wild-type, FUS-R518K and FUS-R521C, respectively, and examined the change in the expression and distribution pattern of FUS by IF and western blot (Figure 4a–d). The overexpression of Drosha S300A/S302A resulted in the cytoplasmic mislocalization of Drosha in HEK293T cells, which contrasts with its nuclear expression and activity (Figure 4a, third column from left). By IF, we found that increasing the levels of the inactive, phospho-dead Drosha ameliorated the sequestration of mutant FUS (R518K and R521C) into the cytoplasmic inclusions as compared to cells expressing mutant FUS alone (Figure 4a). The percentage number of cells with cytoplasmic FUS puncta also showed a significant and robust decrease with Drosha S300A/S302A overexpression in the FUS-R518K and FUS-R521C transfected groups (Figure 4b). In comparison, FUS WT showed no significant changes in its localization with or without Drosha S300A/S302A (Figure 4a and b). In addition, we performed western blot to probe the effect of Drosha S300A/S302A overexpression on the overall levels of wild-type and mutant FUS protein (R518K and R521C) in HEK293T cells. We found that elevated levels of inactive Drosha (S300A/S302A) drastically and significantly reduced FUS protein levels in cells expressing wild-type and mutant FUS compared to FUS-alone groups (Figure 4c and d). In comparison, when we overexpressed EGFP-tagged Drosha in HEK293T cells expressing wild-type and mutant FUS (R518K and R521C), we found a drastic increase in mutant FUS sequestration into the G3BP-positive cytoplasmic inclusions compared to EGFP controls (Figure 4e). Correspondingly, overexpression of Drosha in HEK293T cells resulted in significantly higher endogenous FUS protein compared to EGFP control (Supplementary Figure S5). Similarly, a significant increase in the expression of HA-FUS protein was observed in cells co-transfected with Drosha-GFP and HA-FUS (wild-type and mutant) constructs compared with EGFP controls (Figure 4f and g). Taken together, these findings suggest that Drosha activity might be essential for FUS expression and subcellular localization.

Small RNA profiling revealed novel microRNAs involved in FUS pathogenesis

Global misregulation of miRNA biogenesis has been found as one of the molecular facets of ALS (69,70). Since Drosha is the global regulator of miRNA biogenesis and its interaction with FUS facilitates the synthesis of various neuronal-specific miRNAs (30), we used the small RNA profiling approach to identify the key Drosha-dependent miRNAs that are critical for FUS function and turnover independent of 3′UTR. As in the present study, Drosha showed a robust interaction with FUS-R521C and significantly modulates its expression and mislocalization, we included FUS WT and FUS-R521C for the miRNA profiling studies. The small RNAs were isolated from DKO and HEK293T cells transfected with wild-type and FUS-R521C cDNA constructs, and miRNA transcriptome was profiled and mapped to the human reference genome and other snRNA databases (Figure 5a). By using the *in silico* DESeq2 format, we identified various differentially expressed (DE) miRNAs in different pairwise comparisons using adjusted P value threshold of ≤ 0.01 and a log-fold change of ≥ 1.5 (Figure 5b). We found 695 differentially expressed miRNAs (553 upregulated and 142 downregulated) in FUS-R521C expressing DKO cells in contrast to 41 in FUS-R521C expressing HEK293T cells (31 upregulated and 11 downregulated) when compared to the control groups (Figure 5b). Similarly, heat maps of the top 40 DE miRNAs in FUS-R521C showed a contrasting trend in DKO and HEK293T cells when compared to control groups (Figure 5c, Supplementary Figure S6), suggesting that mutant FUS-R521C expression in the absence of Drosha could influence the miRNA expression profile. Interestingly, we found six distinct and differentially expressed miRNAs (three upregulated and three downregulated) when we compared the FUS-R521C vs control group in DKO cells with the FUS-R521C vs control group in HEK293T cells (Figure 5d). To validate the miRNA sequencing results, we chose top-hit miRNAs from the up- (miR-6832–5p) and down-regulated (miR-378i) groups and examined their expression pattern in FUS-expressing cells with or without Drosha using the TaqMan qPCR assay. After normalization with U6 snRNA, we found a significant and robust decrease in miR-378i and increase in miR-6832–5p levels in DKO cells expressing FUS WT and FUS-R521C as compared to the HEK293T control groups (Figure 5e and f). Interestingly, the levels of miR-378i showed a significant increase in FUS-R521C-expressing HEK293T cells as compared to FUS WT and control groups (Figure 5e). We validated our findings in CRISPR/Cas9-edited human FUS iPSC neurons and examined miR-378i and miR-6832–5p levels relative to isogenic control by real-time PCR. While the levels of miR-378i remained unchanged, we found a significant reduction in miR-6832–5p levels in differentiated FUS-P525L neurons as compared to isogenic control (Supplementary Figure S7). Overall, these results demonstrate that Drosha-dependent miRNAs might be affected by FUS mutations and could potentially modulate FUS expression independently of 3′UTR.

Mapping protective effects of microRNAs in FUS iPSC neurons

To investigate whether reduced miR-378i or increased miR-6832–5p activity affects the expression of ALS-linked FUS mutants, we modulated the levels of these miRNAs in FUS-P525L neurons or stably expressing FUS-N2a cells using custom synthesized, Cy3-labeled antagomiR-378i and miR-6832–5p mimic (Figure 6a), respectively, and analyzed FUS mRNA and protein levels. The antagomiR-378i and miR-6832–5p mimic were validated by qPCR in HEK293T cells (Figure 6b and c). Intriguingly, we found a significant reduction in FUS protein levels by either suppressing miR-378i activity or upregulating miR-6832–5p levels in FUS-P525L and isogenic control neurons (Figure 6d and e), implying a possible direct-correlation between FUS expression and miR-378i activity, while miR-6832–5p might exert an inverse interdependence with FUS. Furthermore, we performed similar experiments in N2a cells expressing FUS WT, R521C and P525L under a DOX-inducible system (Figure 6f and g), as well as in HEK293T cells transfected with wild-type and mutant FUS (R518K and R521C) (Supplementary Figure S8) and found a significant decrease in FUS protein levels by antagomir-miR-378i, miR-6832–5p mimic (Figure 6g and Supplementary Figure S8) or both (Figure 6g). On the contrary, increasing miR-378i or reducing miR-6832–5p levels caused a significant upregulation in FUS protein levels in HEK293T cells co-transfected with FUS (WT, R518K and R521C) and either miR-378i mimic or antagomir-6832–5p (Supplementary

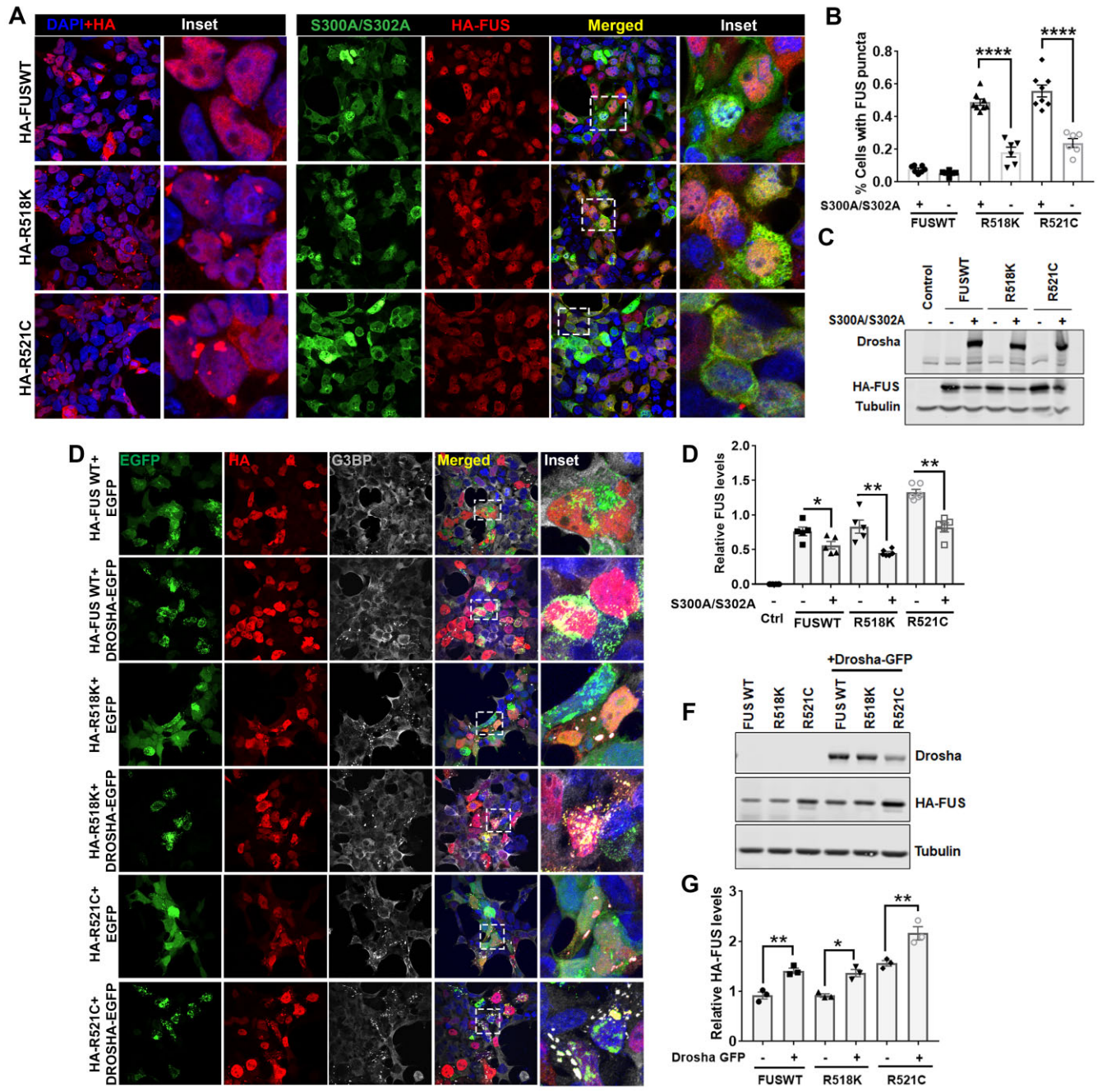

Figure 4. Decreasing Drosha activity prevents mutant FUS aggregation. (**A**) Representative IF images of cytoplasmic FUS aggregation in HEK cells transfected with HA-FUS, HA-R518K and HA-R521C (left two columns) and when cotransfected with phospho-dead Drosha with a serine to alanine change at position 300/302 (four columns from the right). Inset images showed a strong reduction in the cytoplasmic mutant FUS puncta by DROSHA S300A/S302A overexpression (right column) as compared to controls (second column from left). (**B**) Bar graph quantification showing a significant reduction in the percentage of cells with FUS puncta by DROSHA S300A/S302A when co-expressed with FUSWT, R518K and R521C. Cells co-expressing FUS and cytoplasmic mutant Drosha from 6–8 confocal images were used for the quantification ($n = 6$–8, two-tailed unpaired *t*-test). (**C**) Representative immunoblots of HA-FUS levels in HEK293T cell lysates transfected with HA-tagged wild-type (WT) and mutant FUS (R518K and R521C) with or without DROSHA S300A and S302A. Tubulin was used as a normalization control. (**D**) Bar graph showing that HA-FUS levels was significantly decreased in cells co-expressing DROSHA S300A/S302A and HA-tagged FUS (WT, R518K and R521C) as compared to FUS alone ($n = 3$, two-tailed unpaired *t*-test). (**E**) Representative IF images of HEK cells transfected with WT and mutant FUS (HA-R518K and HA-R521C) in combination with either control EGFP or DROSHA-GFP. Inset images showing a strong aggravation of cytoplasmic FUS puncta with DROSHA overexpression as compared to EGFP controls. (**F**) Representative immunoblots of HA-FUS levels in HEK cells co-transfected with HA-FUS constructs (WT, R518K and R521C) and either DROSHA-GFP or EGFP control constructs. (**G**) Bar plot showing a significant increase in HA-FUS levels by DROSHA overexpression in cells co-expressing FUS constructs as compared to EGFP controls ($n = 3$, two-tailed unpaired *t*-test). All microscopic images were taken at 60 optical magnification, and DAPI was used to mark the nucleus. The data (B, D and G) represent mean ± SEM. *P* values (****<0.0001, **<0.01, *≤ 0.05).

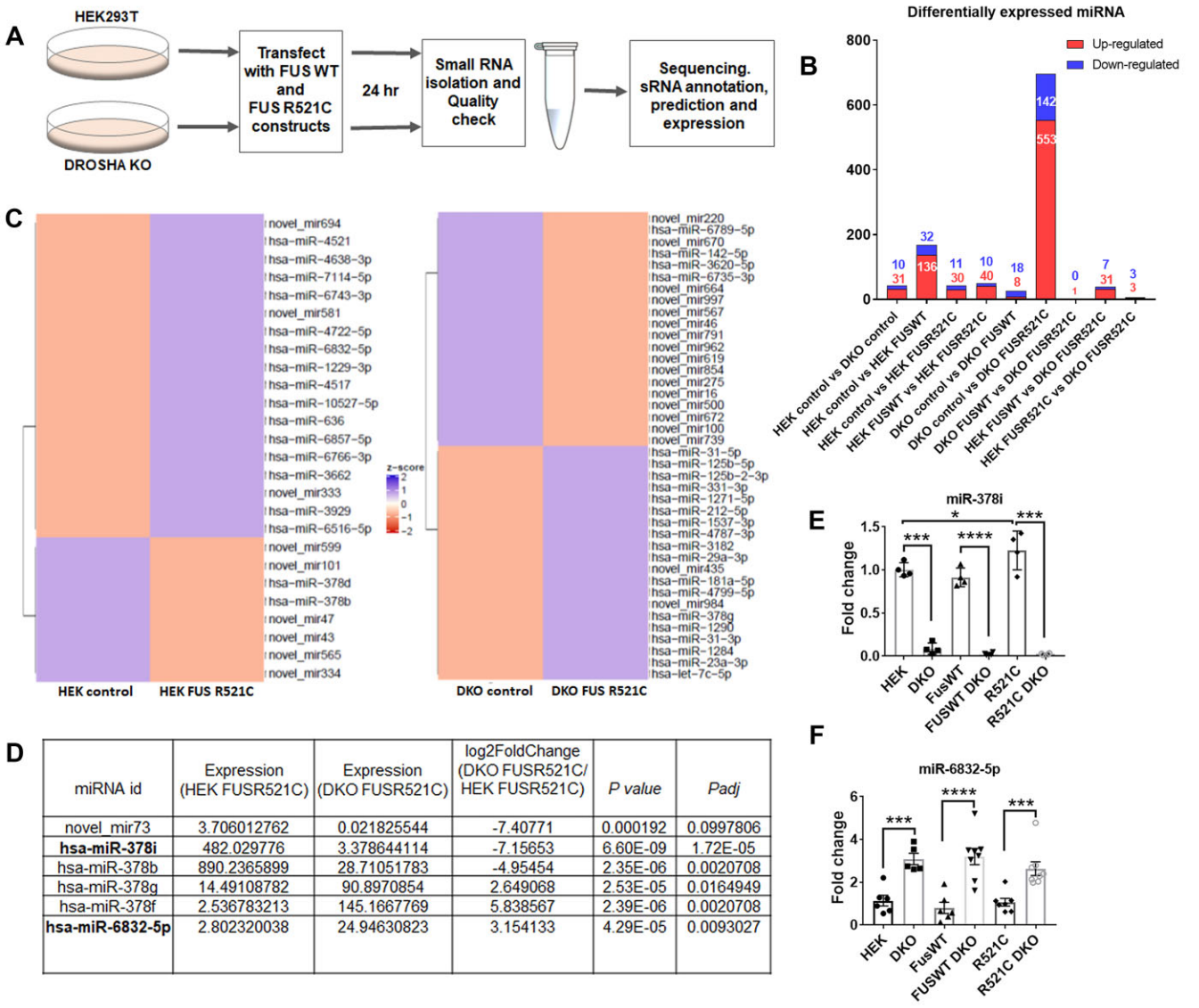

miRNA id	Expression (HEK FUSR521C)	Expression (DKO FUSR521C)	log2FoldChange (DKO FUSR521C/ HEK FUSR521C)	*P value*	*Padj*
novel_mir73	3.706012762	0.021825544	-7.40771	0.000192	0.0997806
hsa-miR-378i	482.029776	3.378644114	-7.15653	6.60E-09	1.72E-05
hsa-miR-378b	890.2365899	28.71051783	-4.95454	2.35E-06	0.0020708
hsa-miR-378g	14.49108782	90.8970854	2.649068	2.53E-05	0.0164949
hsa-miR-378f	2.536783213	145.1667769	5.838567	2.39E-06	0.0020708
hsa-miR-6832-5p	2.802320038	24.94630823	3.154133	4.29E-05	0.0093027

Figure 5. Small RNA profiling of Drosha-dependent micro-RNAs in mutant FUS. (**A**) Schematic representation of the workflow from the sample preparation to small RNA sequencing. (**B**) Bar-graph representation of differentially expressed microRNAs among nine different pairwise comparisons (control vs DKO, control vs FUS WT, control vs FUS R521C, FUSWT vs FUS R521C, DKO control vs DKO FUS WT, DKO control vs DKO FUS R521C, DKO FUS WT vs DKO FUS R521C and HEK FUS R521C vs DKO FUS R521C). (**C**) Heat map depicting the differentially expressed miRNAs in FUS-R521C compared to controls with or without Drosha in HEK293T cells. (**D**) Table of miRNAs with FDR adjusted *P* values 0.05 that are up- or down-regulated in DKO cells expressing FUS-R521C versus HEK293T cells transfected with FUS-R521C. (**E**,**F**) QPCR validation of miR-378i and miR-6832–5p levels as in the table in (**D**) in FUSWT, R521C and un-transfected control with or without Drosha. The data represent mean ± SEM. *P* values (****<0.0001, ***<0.001, *≤0.05).

Figure S9). Correspondingly, we found a significant decrease in FUS mRNA levels in FUS-P525L and isogenic control neurons by antagomir-378i and miRNA-6832–5p mimic, indicating that FUS could be the potential target of these miRNAs (Figure 6h). Furthermore, to determine whether FUS is the possible target of these miRNAs, we checked for the presence of any putative target sites of these miRNAs in FUS by *in silico* TargetScan analysis. We found a single responsive element that is complementary to the canonical 7-mer miR-6832–5p seed sequence in the 3′UTR region of FUS (Supplementary Figure S10). Furthermore, on account of the low conservation context score of the miR-6832–5p seed sequence with the FUS 3′UTR, we speculated on the possibility of an indirect effect of miR-6832–5p on FUS expression. Among all the possible targets identified in our small RNA profiling, we found a putative target of miR-6832–5p, Ribosomal L1 domain containing 1 (RSL1D1), which has been shown as a possible interactor of FUS(71). The miR-6832–5p has three binding elements in the 3′UTR of RSL1D1 mRNA (Supplementary Figure S10). By qPCR, we found a significant decrease in RSL1D1 mRNA levels in P525L neurons transfected with miR-6832–5p mimic compared to isogenic control (Figure 6i), suggesting a similar inverse correlation of miR-6832–5p expression with RSLD1 levels as of FUS. To analyze the interrelationship of FUS, RSL1D1 and miR-6832–5p, we evaluated the RSL1D1 mRNA expression in HEK293T cells transfected with wild-type and mutant FUS (R518K and R521C) with or without Drosha. Compared to FUSWT and controls, RSL1D1 mRNA

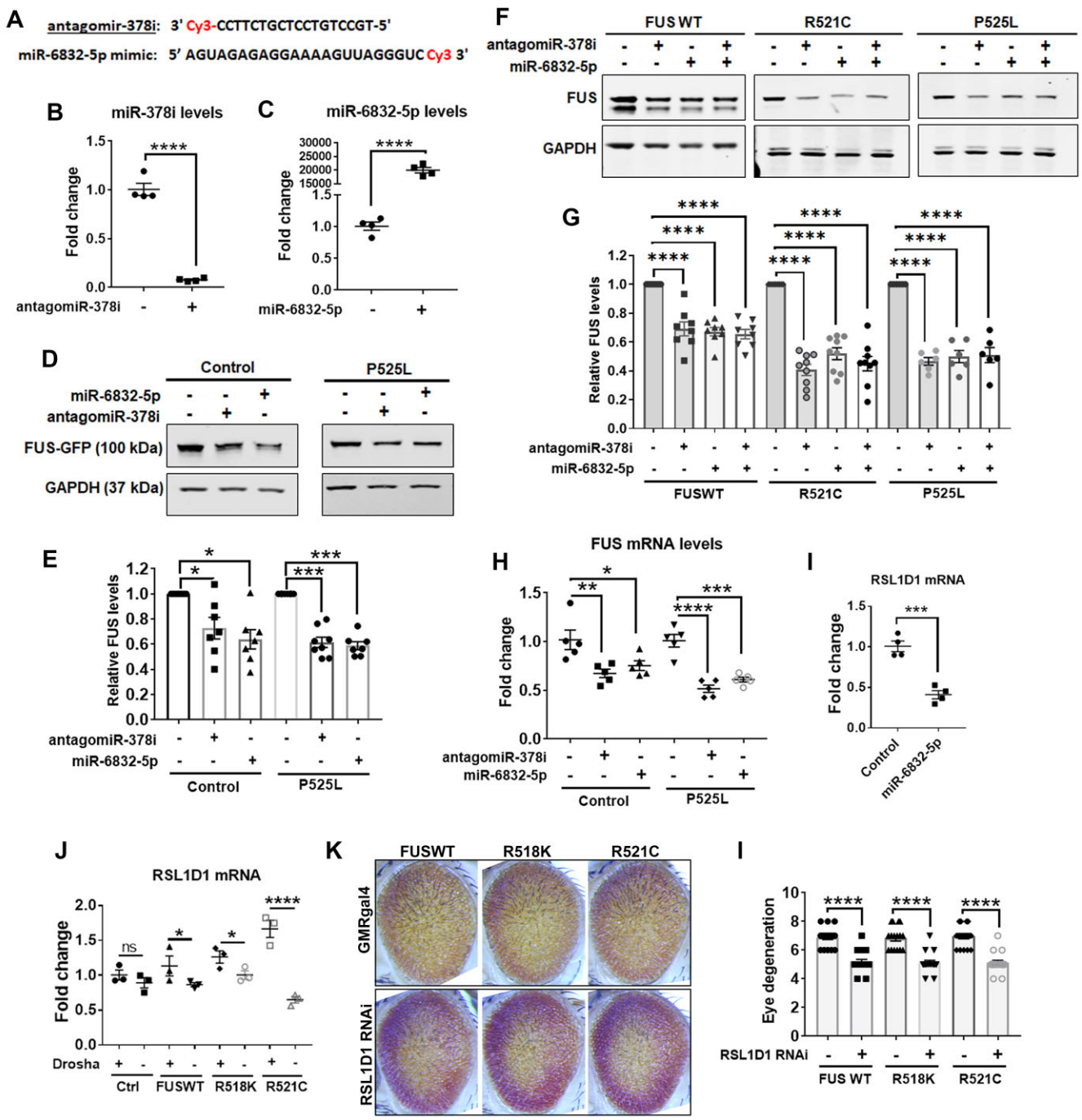

Figure 6. miR-6832–5p and miR-378i regulate FUS expression. (**A**) Ribonucleotide sequences of custom-synthesized miR-6832–5p mimic and antagomiR-378i. (**B**,**C**) qPCR validation of miR-6832–5p and miR-378i levels in HEK293T cells following transfection with miR-6832–5p mimic (**B**) and antagomiR-378i (**C**), respectively ($n = 4$, two-tailed unpaired *t*-test). (**D**) Representative immunoblots of FUS protein expression in isogenic controls and mutant FUS-P525L neurons after transfection with miR-6832–5p mimic and antagomiR-378i. GAPDH was used as internal control. (**E**) Bar graph showing a significant decrease in FUS protein levels by overexpression of miR-6832–5p or inhibition of miR-378i in mutant FUS-P525L neurons as compared to isogenic controls ($n = 7$, one way ANOVA). (**F**) Representative immunoblots demonstrating the levels of FUS after treatment with miR-6832–5p mimic, antagomir-378i or both in DOX-induced FUS WT, FUS R521C and FUS P525L N2a cells. (**G**) Scatter bar graph showing the significant decrease in the levels of wild-type and mutant FUS (R521C and P525L) in N2a cells as in (**F**) by miR-6832–5p mimic, antagomir-378i or both ($n = 8$, one way ANOVA). (**H**) QPCR of total RNA from isogenic control and FUS-P525L neurons revealed a significant decrease in FUS levels in neurons transfected with miR-6832–5p mimic or miR-378i inhibitor, respectively, as compared to untransfected controls ($n = 4$, two-tailed unpaired *t*-test). (**I**) Bar plot of target validation by qPCR showing a decrease in RSL1D1 mRNA levels by miR-6832–5p ($n = 4$, two-tailed unpaired *t*-test). (**J**) qPCR of RNA isolated from DKO cells expressing WT and mutant FUS showed a significant reduction in RSL1D1 mRNA as compared to HEK293T controls ($n = 3$, two-tailed unpaired *t*-test). (**K**) Representative eye images of flies expressing WT and mutant FUS transgene either alone or in combination with RNAi-mediated knockdown of RSL1D1. (**L**) Bar plot depicting that RSL1D1 knockdown significantly reduces FUS-mediated eye degeneration in WT and mutant FUS flies ($n = 16$, two-tailed unpaired *t*-test). The data (B, C, E, G, H, I, J and L) represent mean ± SEM. *P* values (****<0.0001, ***<0.001, *<0.01, *≤0.05).

levels were significantly increased in FUS-R518K and FUS-R521C expressing cells, and its levels showed a significant reduction in the absence of Drosha (Figure 6j). To further probe the genetic and functional link between FUS and RSL1D1, we assessed the effect of RNAi-mediated knockdown of RSL1D1 on mutant FUS-linked eye degeneration *in vivo* (Figure 6k). Compared to WT and mutant FUS (R518K and R521C) expressing flies, we found a significant decrease in FUS-mediated eye degeneration on RSL1D1 depletion (Figure 6k and l), suggesting that RSL1D1 could be a possible modulator of FUS toxicity, thereby, establishing a feasible interdependence between RSL1D1, FUS and miR-6832–5p activity.

miR-378i suppresses G3BP1-mediated stress granule formation and modulates mutant FUS solubility

Since the sequestration of mutant FUS into insoluble cytoplasmic inclusions is known to cause neuronal toxicity and death, we evaluated the effect of miR-378i and miR-6832–5p activity on the FUS solubility in neuronal cells. First, we examined if the mutant FUS caused the segregation of miR-378i and miR-6832–5p in the soluble and insoluble RNA fractions of DOX-induced FUSWT, FUS-R521C and FUS-P525L N2a cells by qPCR (Figure 7a and b). We found a significant 2- to 4-fold increase in miR-378i levels in the insoluble fraction of R521C and P525L cells, whereas FUSWT showed no apparent change in the miRNA levels (Figure 7a). On the contrary, miR-6832–5p showed a significant decrease in the insoluble fraction of P5252L with no change in FUSWT and R521C cells (Figure 7b), suggesting that mutant FUS may lead to differential and abnormal sequestration of miRNAs in the cytoplasmic insoluble inclusions. Next, we tested whether altering the levels of miR-378i and miR-6832–5p affects the solubility of FUS protein. We transfected FUS-P525L and isogenic control neurons with either antagomir-378i or miR-6832–5p mimic and measured the levels of FUS protein in the soluble and insoluble lysates. We found that both antagomir-378i and miR-6832–5p mimic caused a significant reduction in the insoluble FUS protein in P525L neurons as compared to the isogenic controls (Figure 7c and d). Likewise, we investigated the effect of miR-378i and miR-6832–5p activity on the protein solubility of other two FUS mutants, FUS-R518k and FUS-R521C, in HEK293T cells and found that the absence of miR-378i activity significantly abated the levels of insoluble mutant FUS protein (Figure 7e and f) whereas increased miR-6832–5p activity was required to improve FUS solubility (Figure 7e and g). Furthermore, we probed the role of miR-378i and miR6832-5p in the sequestration of mutant FUS into insoluble cytoplasmic stress granules by IF. We introduced antagomir-378i and miR6832-5p mimic into the Dox-induced R521C cells and assessed the change in FUS solubility and localization under stress condition (Figure 7h and i). We found that antagomir-378i significantly ameliorated insoluble FUS inclusions in the cytoplasm. Notably, the cells with higher levels of antagoimiR-378i showed a significant reduction in FUS R521C level, suggesting that the dosage of miRNA-378i is crucial for mutant FUS expression and its aggregation (Figure 7h and j). We found equivalent results when we overexpress miR-6832–5p and found a significant decrease in R521C intensity and its cytoplasmic aggregation in N2a cells (Figure 7i and k). Interestingly, we found that reducing miR-378i levels significantly prevent G3BP-mediated stress granule formation, suggesting that miR-378i could be involved in the buildup of insoluble FUS inclusions by modulating the stress granule assembly (Figure 7h, l and Supplementary Figure S11). However, miR-6832–5p has no apparent effect on G3BP-mediated stress granules, suggesting that it might regulate FUS levels and solubility via some other mechanism (Figure 7i and l). Overall, these findings indicate that mutant FUS expression and its toxic cytoplasmic segregation could be regulated by altering the activity of various Drosha-dependent miRNAs.

Discussion

Our findings demonstrate a strong correlation between Drosha and microRNAs expression with FUS levels, its solubility, and the abnormal segregation of mutant FUS in the cytoplasm. Disease causing mutation in FUS have been linked with clinically heterogeneous and aggressive forms of ALS (71–74). With previous unbiased deficiency screen in *Drosophila* (45) combined with the knockdown studies, we identified Drosha as one of the strong suppressors of FUS-mediated degeneration and neuronal defects. Drosha is the core ribonuclease of miRNA processing pathway responsible for generating microRNA precursors (pre-miRNAs) in the nucleus (40,41,75). Drosha has been extensively studied for its cell-type specific expression (49), posttranscriptional modifications (76), degradation (77) and for its importance in RNA metabolism (78), development, differentiation and regulation of neurogenesis (79,80). However, it has never been directly implicated with ALS pathogenesis. We performed comprehensive studies in *Drosophila* to demonstrate that targeted depletion of Drosha can sufficiently mitigate FUS-mediated neurodegeneration (Figure 1). We found that knockdown of Drosha significantly attenuated eye degeneration and developmental eclosion defects, as well as motor neuron-related locomotion and climbing defects caused by wild-type and mutant FUS expression in flies. Interestingly, we found a direct correlation between Drosha and FUS levels. The reduction of Drosha in motor neurons of flies caused a significant decrease in the levels of FUS and it was further validated in CRISPR/Cas9 generated DKO HEK293 cells (Figure 3c). Intriguingly, we found that Drosha affects FUS protein levels independently of the 3′UTR (Figure 3c and Supplementary Figure S3) and its reduction strongly abated the stability of overexpressed FUS WT and R521C (Figure 3h–m). This suggests that Drosha may regulate FUS levels by modulating its interaction and rate of degradation (Figures 2 and 3). Furthermore, the reduced levels of Drosha significantly improved the life span of FUS expressing flies, further supporting our findings that Drosha is a strong modulator of FUS activity and toxicity.

Drosha assembles in a large protein complex, known as the Drosha Microprocessor complex, in association with DGRC8 and multiple auxiliary factors such as RNA helicases (p68, p72 and DHX9) and hnRNPs (hnRNP R, hnRNP H1 and hnRNPU) which together modulate the binding efficacy, fidelity and cleavage specificity of Drosha (39,81). Recently, FUS has been identified as one of the interactors and regulator of Drosha-mediated miRNA biogenesis (39). FUS facilitates the generation of subset of miRNAs by binding and recruiting Drosha at pri-miRNA chromatin loci (29,30). The direct implication of mutant FUS that manifests as toxic protein aggregates on Drosha expression and activity is not well studied in ALS pathogenesis. We found that mutant FUS (R521C) showed a strong

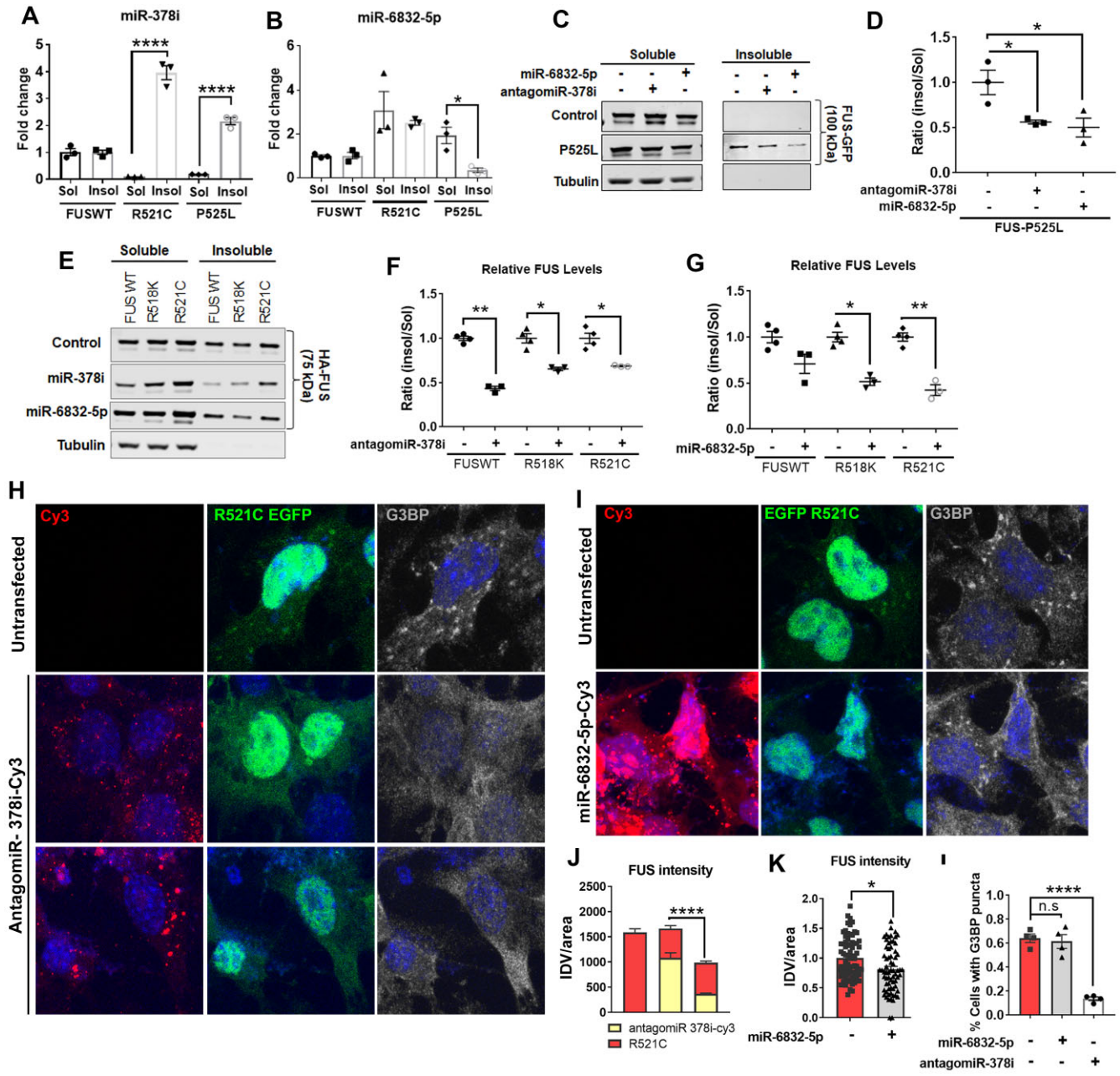

Figure 7. Overexpression of miR-6832–5p and inhibition of miR-378i promote FUS solubility and prevent its cytoplasmic aggregation. (**A**,**B**) Bar graphs showing the fold change in the mature miRNA levels of miR-378i (**A**) and miR-6832–5p (**B**) in the soluble and insoluble fractions of total RNA isolated from DOX-induced FUS WT, FUS R521C and FUS P5252L N2a cells ($n = 3$, two-tailed unpaired *t*-test). (**C**) Representative immunoblots presenting the soluble and insoluble fractionation of FUS protein in FUS-P525L and isogenic control neurons when transfected with miR-6832–5p mimic and antagomir-378i. (**D**) Bar graph quantification of ratio of insoluble to soluble levels of FUS as in panel (**C**), showing a significant reduction in insoluble FUS levels in FUS-P525L transfected with miR-6832–5p mimic and antagomiR-378i as compared to control neurons ($n = 3$, two-tailed unpaired *t*-test). (**E**) Representative blots of soluble and insoluble fractionation of FUS from HEK293T cell cotransfected with FUS constructs (WT, R518K and R521C) and miR-6832–5p mimic or antagomiR-378i. (**F**, **G**) Bar graphs representing the significant decrease in insoluble FUS levels by miR-378i inhibition (**F**) and miR-6832–5p overexpression (**G**) in cells expressing WT and mutant FUS. Soluble tubulin levels were used as normalization control ($n = 4$, two-tailed unpaired *t*-test). The data represent mean ± SEM. *P* values (****<0.0001, **<0.01, *<0.05). (**H**) Representative IF images of DOX-induced and sodium arsenite-treated R521C-N2a cells transfected with antagomir-378i for 48 hours. The lower two panels depict the effect of heterogenous transfection (low and high) of antagomir-378i on FUS levels and cytoplasmic G3BP-puncta compared to controls (**I**) Representative IF images of DOX-induced and sodium arsenite-treated FUS R521C-N2a cells depicting the decrease in FUS expression when transfected with miR-6832–5p. (**J**) Bar plot showing significant decrease in FUS expression with different transfected levels of antagomir-378i as shown in (**H**) ($n = 25$–35, two-tailed unpaired *t*-test). (**K**) Bar graph showing that overexpression of miR-6832–5p significantly decrease FUS levels as in (**I**) ($n = 76$, two-tailed unpaired *t*-test). (**L**) Bar plot indicating a significant reduction in the number of G3BP-positive stress granule puncta by antagomir-378i in DOX-induced FUS R521C as shown in (H). Four x60 microscopic images were used for the quantification ($n = 4$, two-tailed unpaired *t*-test), and DAPI was used to mark the nucleus. The data (A, B, D, F and G) represent mean ± SEM. *P* values (****<0.0001, **<0.01, *≤0.05).

interaction with Drosha and caused its abnormal sequestration in the cytoplasmic FUS inclusion (Figure 2b and c). Moreover, Drosha showed a strong nuclear/cytoplasmic partitioning under stress condition and accumulates in G3BP-positive cytoplasmic stress granule (Figure 2d). Previous studies have shown that stress causes P38MAPK-mediated phosphorylation of Drosha which prevents its interaction with DGCR8 and promotes its nuclear export and degradation (82). Thus, we can deduce that disease causing FUS mutations may influence Drosha function by altering its expression and subcellular localization.

The unbalanced nuclear/cytoplasmic partitioning and entrapment of mutant FUS in the cytoplasmic stress granules is a well-established hallmark of ALS-FUS pathogenesis (21). We demonstrated that depletion of Drosha in *Drosophila* brain and HEK293T cells led to decrease cytoplasmic mutant FUS inclusions, and this effect is dependent on Drosha levels and activity (Figure 3a and f). Drosha activity and its nuclear import is dependent on its phosphorylation at 300 and 302 Serine residues (68). We found that overexpression of phospho-dead Drosha with Serine to Alanine change at 300/302 residue in HEK-293T cells prevents the aggregation of mutant FUS in cytoplasm and cause a significant decrease in FUS levels (Figure 4a). Together, these results indicates that reduction in Drosha activity seems essential for dispersing abnormal mutant FUS aggregates.

Drosha is a core protein for microRNA biogenesis and a variety of microRNAs are essential for the functioning of the nervous system and the development and survival of neurons (39,69,79). Dysregulation of miRNA networks have been linked with various neurodegenerative diseases, including ALS and Alzheimer's disease (AD) (69,83–85). FUS via its interaction with Drosha is shown to facilitate synthesis of various neuronal-specific miRNAs, with an essential role in neuronal differentiation and synaptogenesis (42,69). To comprehensively assess the detrimental effect of disease-causing FUS mutations on global microRNA biogenesis and to identify various miRNAs misregulated and involved in Drosha-mediated suppression of FUS toxicity independent of 3′UTR, we expressed wild-type and mutant FUS R521C cDNA constructs in the control and CRISPR/Cas9 generated DKO HEK293 cells and performed microRNA profiling by high throughput RNA sequencing. Intriguingly, we found six Drosha-regulated microRNAs that are differentially expressed in mutant FUS-R521C (Figure 5). Of these, we further evaluated the role of miR-378i and miR-6832–5p in context of mutant FUS toxicity in mouse N2a cells as well as in CRISPR/Cas9 generated FUS P525L iPSC neurons. miR-378i levels showed a significant decrease in FUS-R521C expressing DKO cells whereas miR-6832–5p was highly upregulated upon Drosha depletion, suggesting that mutant FUS-R521C has a contrasting effect on the expression of these Drosha-dependent miRNAs. miR-378 family of microRNAs have been implicated in various forms of cancer as well as neuronal autophagy and neurological functional impairment (86), however, the role of miR-378i and miR-6832–5p is still not well established. We found that modulating the levels of miR-378i and miR-6832–5p has contrasting effect on the expression, localization and solubility of mutant FUS in N2a and FUS-P525L neurons. The levels of miR-378i were significantly elevated in the insoluble RNA fraction of mutant FUS (R521C and P5252L) expressing N2a cells whereas miR-6832–5p levels are significantly lower in the insoluble RNA fraction of FUS-P525L cells, suggesting a distinctive mode of action of the two miRNAs in FUS-mediated toxicity (Figure 7a and b). We used custom-synthesized antagomir-378i and miR-6832–5p mimic to determine the effect of these miRNAs on FUS levels, localization, and solubility. Our data suggested that depletion of miR-378i led to decrease in FUS mRNA and protein levels, prevents the toxic segregation of mutant FUS into the cytoplasmic G3BP-positive stress granules and significantly decrease the insolubility of mutant FUS. On the contrary, we found that miR-6832 overexpression is required to ameliorate FUS levels, mutant FUS solubility and its cytoplasmic aggregation. *In silico* target analysis showed a single putative target site of miR-6832–5p on the 3′UTR region of FUS, suggesting the possibility of FUS being the direct target of miR-6832–5p. In addition, among various presumed targets of miR-6832–5p, we found RSL1D1 (also validated by qPCR), which is a known putative interactor of FUS (71) and found a possible link between mutant FUS toxicity with the miR-6832–5p target-RSL1D1 (Supplementary Figure S4). We found that depletion of Drosha significantly decrease the levels of RSL1D1, which is contrary to the increased levels of miR-6832–5p on DKO. Additionally, we found that decrease in RSL1D1 levels significantly alleviated FUS mediated eye toxicity in flies. These data suggest that miR-6832–5p may regulate FUS activity through different molecules and pathways. On the other hand, we found that antagomiR-378i impedes mutant FUS aggregation by preventing the G3BP-mediated stress granule formation, and since miR-378i showed less target similarly with FUS, we suggest a possible indirect mode of regulation of mutant FUS toxicity by miR-378i (Figure 7h).

Overall, our study established Drosha as a potential modifier of FUS-mediated neurodegeneration and revealed a differential miRNA-based regulation of FUS activity and solubility. With this work, we elaborated that Drosha and FUS activities are interdependent and disease-causing FUS mutations disrupt microRNA biogenesis. We provided compelling evidence highlighting alternate miRNA-linked molecular mechanisms in modulating pathogenic FUS mediated neurodegeneration in ALS.

Data availability

The data underlying this article are available in the Gene Expression Omnibus at https://www.ncbi.nlm.nih.gov/geo/, and can be accessed under accession code GSE242360.

Supplementary data

Supplementary Data are available at NAR Online.

Acknowledgements

Author contributions: Design of this study: S.K., T.R.F., E.N.A., D.M., J.B., R.S., C.W., R.R., D.R., J.S. and U.B.P.; Wrote the manuscript: S.K., U.B.P.; Critically read and edited the manuscript: S.K., E.N.A. and U.B.P. All authors reviewed and approved the manuscript prior to submission.

Funding

This work has been supported by National Institute of Health (NIH) grant R01NS081303 to U.B.P. This research was supported in part by the HTC cluster from the University of

Pittsburgh Center for Research Computing, which is supported by NIH award number S10OD028483.

Conflict of interest statement

None declared.

References

1. Nussbacher,J.K., Tabet,R., Yeo,G.W. and Lagier-Tourenne,C. (2019) Disruption of RNA metabolism in neurological diseases and emerging therapeutic interventions. *Neuron*, **102**, 294–320.
2. Gerstberger,S., Hafner,M. and Tuschl,T. (2014) A census of human RNA-binding proteins. *Nat. Rev. Genet.*, **15**, 829–845.
3. Lunde,B.M., Moore,C. and Varani,G. (2007) RNA-binding proteins: modular design for efficient function. *Nat. Rev. Mol. Cell Biol.*, **8**, 479–490.
4. Conlon,E.G. and Manley,J.L. (2017) RNA-binding proteins in neurodegeneration: mechanisms in aggregate. *Genes Dev.*, **31**, 1509–1528.
5. Arai,T., Hasegawa,M., Akiyama,H., Ikeda,K., Nonaka,T., Mori,H., Mann,D., Tsuchiya,K., Yoshida,M., Hashizume,Y., *et al.* (2006) TDP-43 is a component of ubiquitin-positive tau-negative inclusions in frontotemporal lobar degeneration and amyotrophic lateral sclerosis. *Biochem. Biophys. Res. Commun.*, **351**, 602–611.
6. Winton,M.J., Igaz,L.M., Wong,M.M., Kwong,L.K., Trojanowski,J.Q. and Lee,V.M. (2008) Disturbance of nuclear and cytoplasmic TAR DNA-binding protein (TDP-43) induces disease-like redistribution, sequestration, and aggregate formation. *J. Biol. Chem.*, **283**, 13302–13309.
7. Panoutsopoulou,K., Metrustry,S., Doherty,S.A., Laslett,L.L., Maciewicz,R.A., Hart,D.J., Zhang,W., Muir,K.R., Wheeler,M., Cooper,C., *et al.* (2014) The effect of FTO variation on increased osteoarthritis risk is mediated through body mass index: a Mendelian randomisation study. *Ann. Rheum. Dis.*, **73**, 2082–2086.
8. Neumann,M., Sampathu,D.M., Kwong,L.K., Truax,A.C., Micsenyi,M.C., Chou,T.T., Bruce,J., Schuck,T., Grossman,M., Clark,C.M., *et al.* (2006) Ubiquitinated TDP-43 in frontotemporal lobar degeneration and amyotrophic lateral sclerosis. *Science*, **314**, 130–133.
9. Kapeli,K., Martinez,F.J. and Yeo,G.W. (2017) Genetic mutations in RNA-binding proteins and their roles in ALS. *Hum. Genet.*, **136**, 1193–1214.
10. Al-Chalabi,A., van den Berg,L.H. and Veldink,J. (2017) Gene discovery in amyotrophic lateral sclerosis: implications for clinical management. *Nat. Rev. Neurol.*, **13**, 96–104.
11. Filippini,T., Fiore,M., Tesauro,M., Malagoli,C., Consonni,M., Violi,F., Arcolin,E., Iacuzio,L., Oliveri Conti,G., Cristaldi,A., *et al.* (2020) Clinical and lifestyle factors andrisk of amyotrophic lateral sclerosis: a population-based case-control study. *Int. J. Environ. Res. Public Health*, **17**, 857.
12. Ito,D., Hatano,M. and Suzuki,N. (2017) RNA binding proteins and the pathological cascade in ALS/FTD neurodegeneration. *Sci. Transl. Med.*, **9**, eaah5436.
13. Taylor,J.P., Brown,R.H. Jr and Cleveland,D.W. (2016) Decoding ALS: from genes to mechanism. *Nature*, **539**, 197–206.
14. Kwiatkowski,T.J. Jr, Bosco,D.A., Leclerc,A.L., Tamrazian,E., Vanderburg,C.R., Russ,C., Davis,A., Gilchrist,J., Kasarskis,E.J., Munsat,T., *et al.* (2009) Mutations in the FUS/TLS gene on chromosome 16 cause familial amyotrophic lateral sclerosis. *Science*, **323**, 1205–1208.
15. Sreedharan,J., Blair,I.P., Tripathi,V.B., Hu,X., Vance,C., Rogelj,B., Ackerley,S., Durnall,J.C., Williams,K.L., Buratti,E., *et al.* (2008) TDP-43 mutations in familial and sporadic amyotrophic lateral sclerosis. *Science*, **319**, 1668–1672.
16. Dormann,D., Rodde,R., Edbauer,D., Bentmann,E., Fischer,I., Hruscha,A., Than,M.E., Mackenzie,I.R., Capell,A., Schmid,B., *et al.* (2010) ALS-associated fused in sarcoma (FUS) mutations disrupt Transportin-mediated nuclear import. *EMBO J.*, **29**, 2841–2857.
17. Ramesh,N., Kour,S., Anderson,E.N., Rajasundaram,D. and Pandey,U.B. (2020) RNA-recognition motif in Matrin-3 mediates neurodegeneration through interaction with hnRNPM. *Acta Neuropathol Commun*, **8**, 138.
18. Kim,H.J. and Taylor,J.P. (2017) Lost in transportation: nucleocytoplasmic transport defects in ALS and other neurodegenerative diseases. *Neuron*, **96**, 285–297.
19. Midura-Nowaczek,K., Bruzgo,I., Radzajewska,B., Roszkowska-Jakimiec,W. and Worowski,K. (1988) (Synthesis and antifibrinolytic activity of dipeptides of E-aminocaproic acid and sulfur-containing amino acids.). *Acta Pol. Pharm.*, **45**, 35–41.
20. Liu,Y.J., Kuo,H.C. and Chern,Y. (2021) A system-wide mislocalization of RNA-binding proteins in motor neurons is a new feature of ALS. *Neurobiol. Dis.*, **160**, 105531.
21. Vance,C., Rogelj,B., Hortobagyi,T., De Vos,K.J., Nishimura,A.L., Sreedharan,J., Hu,X., Smith,B., Ruddy,D., Wright,P., *et al.* (2009) Mutations in FUS, an RNA processing protein, cause familial amyotrophic lateral sclerosis type 6. *Science*, **323**, 1208–1211.
22. Mitchell,J.C., McGoldrick,P., Vance,C., Hortobagyi,T., Sreedharan,J., Rogelj,B., Tudor,E.L., Smith,B.N., Klasen,C., Miller,C.C., *et al.* (2013) Overexpression of human wild-type FUS causes progressive motor neuron degeneration in an age- and dose-dependent fashion. *Acta Neuropathol.*, **125**, 273–288.
23. Sabatelli,M., Moncada,A., Conte,A., Lattante,S., Marangi,G., Luigetti,M., Lucchini,M., Mirabella,M., Romano,A., Del Grande,A., *et al.* (2013) Mutations in the 3' untranslated region of FUS causing FUS overexpression are associated with amyotrophic lateral sclerosis. *Hum. Mol. Genet.*, **22**, 4748–4755.
24. Lagier-Tourenne,C., Polymenidou,M., Hutt,K.R., Vu,A.Q., Baughn,M., Huelga,S.C., Clutario,K.M., Ling,S.C., Liang,T.Y., Mazur,C., *et al.* (2012) Divergent roles of ALS-linked proteins FUS/TLS and TDP-43 intersect in processing long pre-mRNAs. *Nat. Neurosci.*, **15**, 1488–1497.
25. Jutzi,D., Campagne,S., Schmidt,R., Reber,S., Mechtersheimer,J., Gypas,F., Schweingruber,C., Colombo,M., von Schroetter,C., Loughlin,F.E., *et al.* (2020) Aberrant interaction of FUS with the U1 snRNA provides a molecular mechanism of FUS induced amyotrophic lateral sclerosis. *Nat. Commun.*, **11**, 6341.
26. Fujii,R., Okabe,S., Urushido,T., Inoue,K., Yoshimura,A., Tachibana,T., Nishikawa,T., Hicks,G.G. and Takumi,T. (2005) The RNA binding protein TLS is translocated to dendritic spines by mGluR5 activation and regulates spine morphology. *Curr. Biol.*, **15**, 587–593.
27. Zinszner,H., Sok,J., Immanuel,D., Yin,Y. and Ron,D. (1997) TLS (FUS) binds RNA in vivo and engages in nucleo-cytoplasmic shuttling. *J. Cell Sci.*, **110**, 1741–1750.
28. Loughlin,F.E., Lukavsky,P.J., Kazeeva,T., Reber,S., Hock,E.M., Colombo,M., Von Schroetter,C., Pauli,P., Clery,A., Muhlemann,O., *et al.* (2019) The solution structure of FUS bound to RNA reveals a bipartite mode of RNA recognition with both sequence and shape specificity. *Mol. Cell*, **73**, 490–504.
29. Zhang,T., Wu,Y.C., Mullane,P., Ji,Y.J., Liu,H., He,L., Arora,A., Hwang,H.Y., Alessi,A.F., Niaki,A.G., *et al.* (2018) FUS regulates activity ofmicroRNA-mediated gene silencing. *Mol. Cell*, **69**, 787–801.
30. Morlando,M., Dini Modigliani,S., Torrelli,G., Rosa,A., Di Carlo,V., Caffarelli,E. and Bozzoni,I. (2012) FUS stimulates microRNA biogenesis by facilitating co-transcriptional Drosha recruitment. *EMBO J.*, **31**, 4502–4510.
31. An,H., Skelt,L., Notaro,A., Highley,J.R., Fox,A.H., La Bella,V., Buchman,V.L. and Shelkovnikova,T.A. (2019) ALS-linked FUS mutations confer loss and gain of function in the nucleus by promoting excessive formation of dysfunctional paraspeckles. *Acta Neuropathol Commun*, **7**, 7.
32. Sahadevan,S., Hembach,K.M., Tantardini,E., Perez-Berlanga,M., Hruska-Plochan,M., Megat,S., Weber,J., Schwarz,P., Dupuis,L., Robinson,M.D., *et al.* (2021) Synaptic FUS accumulation triggers

early misregulation of synaptic RNAs in a mouse model of ALS. *Nat. Commun.*, **12**, 3027.
33. Hock,E.M., Maniecka,Z., Hruska-Plochan,M., Reber,S., Laferriere,F., Sahadevan,M.K.S., Ederle,H., Gittings,L., Pelkmans,L., Dupuis,L., *et al.* (2018) Hypertonic stress causescytoplasmic translocation of neuronal, but not astrocytic, FUS due to impaired transportin function. *Cell Rep.*, **24**, 987–1000.
34. Murakami,T., Qamar,S., Lin,J.Q., Schierle,G.S., Rees,E., Miyashita,A., Costa,A.R., Dodd,R.B., Chan,F.T., Michel,C.H., *et al.* (2015) ALS/FTD mutation-inducedphase transition of FUS liquid droplets and reversible hydrogels into irreversible hydrogels impairs RNP granule function. *Neuron*, **88**, 678–690.
35. Maharana,S., Wang,J., Papadopoulos,D.K., Richter,D., Pozniakovsky,A., Poser,I., Bickle,M., Rizk,S., Guillen-Boixet,J., Franzmann,T.M., *et al.* (2018) RNA buffers the phase separation behavior of prion-like RNA binding proteins. *Science*, **360**, 918–921.
36. Reber,S., Stettler,J., Filosa,G., Colombo,M., Jutzi,D., Lenzken,S.C., Schweingruber,C., Bruggmann,R., Bachi,A., Barabino,S.M., *et al.* (2016) Minor intron splicing is regulated by FUS and affected by ALS-associated FUS mutants. *EMBO J.*, **35**, 1504–1521.
37. Wang,X., Arai,S., Song,X., Reichart,D., Du,K., Pascual,G., Tempst,P., Rosenfeld,M.G., Glass,C.K. and Kurokawa,R. (2008) Induced ncRNAs allosterically modify RNA-binding proteins in cis to inhibit transcription. *Nature*, **454**, 126–130.
38. Zhou,Y., Liu,S., Liu,G., Ozturk,A. and Hicks,G.G. (2013) ALS-associated FUS mutations result in compromised FUS alternative splicing and autoregulation. *PLos Genet.*, **9**, e1003895.
39. Gregory,R.I., Yan,K.P., Amuthan,G., Chendrimada,T., Doratotaj,B., Cooch,N. and Shiekhattar,R. (2004) The Microprocessor complex mediates the genesis of microRNAs. *Nature*, **432**, 235–240.
40. Han,J., Lee,Y., Yeom,K.H., Kim,Y.K., Jin,H. and Kim,V.N. (2004) The Drosha-DGCR8 complex in primary microRNA processing. *Genes Dev.*, **18**, 3016–3027.
41. Lee,Y., Ahn,C., Han,J., Choi,H., Kim,J., Yim,J., Lee,J., Provost,P., Radmark,O., Kim,S., *et al.* (2003) The nuclear RNase III Drosha initiates microRNA processing. *Nature*, **425**, 415–419.
42. Dini Modigliani,S., Morlando,M., Errichelli,L., Sabatelli,M. and Bozzoni,I. (2014) An ALS-associated mutation in the FUS 3'-UTR disrupts a microRNA-FUS regulatory circuitry. *Nat. Commun.*, **5**, 4335.
43. Anderson,E.N., Gochenaur,L., Singh,A., Grant,R., Patel,K., Watkins,S., Wu,J.Y. and Pandey,U.B. (2018) Traumatic injury induces stress granule formation and enhances motor dysfunctions in ALS/FTD models. *Hum. Mol. Genet.*, **27**, 1366–1381.
44. Pucher,J., Jayaprakash,P., Aftyka,T., Sigman,L. and Van Swol,R. (1995) Clinical evaluation of a new flossing device. *Quintessence Int.*, **26**, 273–278.
45. Casci,I., Krishnamurthy,K., Kour,S., Tripathy,V., Ramesh,N., Anderson,E.N., Marrone,L., Grant,R.A., Oliver,S., Gochenaur,L., *et al.* (2019) Muscleblind acts as a modifier of FUS toxicity by modulating stress granule dynamics and SMN localization. *Nat. Commun.*, **10**, 5583.
46. Fortuna,T.R., Kour,S., Chimata,A.V., Muinos-Buhl,A., Anderson,E.N., Nelson Iv,C.H., Ward,C., Chauhan,O., O'Brien,C., Rajasundaram,D., *et al.* (2023) SMN regulates GEMIN5 expression and acts as a modifier of GEMIN5-mediated neurodegeneration. *Acta Neuropathol.*, **146**, 477–498.
47. Nichols,C.D., Becnel,J. and Pandey,U.B. (2012) Methods to assay *Drosophila* behavior. *J. Vis. Exp.*, https://doi.org/10.3791/3795.
48. Lin,Y.C., Kumar,M.S., Ramesh,N., Anderson,E.N., Nguyen,A.T., Kim,B., Cheung,S., McDonough,J.A., Skarnes,W.C., Lopez-Gonzalez,R., *et al.* (2021) Interactions between ALS-linked FUS and nucleoporins are associated with defects in the nucleocytoplasmic transport pathway. *Nat. Neurosci.*, **24**, 1077–1088.
49. Dai,L., Chen,K., Youngren,B., Kulina,J., Yang,A., Guo,Z., Li,J., Yu,P. and Gu,S. (2016) Cytoplasmic Drosha activity generated by alternative splicing. *Nucleic Acids Res.*, **44**, 10454–10466.
50. Marrone,L., Drexler,H.C.A., Wang,J., Tripathi,P., Distler,T., Heisterkamp,P., Anderson,E.N., Kour,S., Moraiti,A., Maharana,S., *et al.* (2019) FUS pathology in ALS is linked to alterations in multiple ALS-associated proteins and rescued by drugs stimulating autophagy. *Acta Neuropathol.*, **138**, 67–84.
51. Fortuna,T.R., Kour,S., Anderson,E.N., Ward,C., Rajasundaram,D., Donnelly,C.J., Hermann,A., Wyne,H., Shewmaker,F. and Pandey,U.B. (2021) DDX17 is involved in DNA damage repair and modifies FUS toxicity in an RGG-domain dependent manner. *Acta Neuropathol.*, **142**, 515–536.
52. Daigle,J.G., Krishnamurthy,K., Ramesh,N., Casci,I., Monaghan,J., McAvoy,K., Godfrey,E.W., Daniel,D.C., Johnson,E.M., Monahan,Z., *et al.* (2016) Pur-alpha regulates cytoplasmic stress granule dynamics and ameliorates FUS toxicity. *Acta Neuropathol.*, **131**, 605–620.
53. Kour,S., Rajan,D.S., Fortuna,T.R., Anderson,E.N., Ward,C., Lee,Y., Lee,S., Shin,Y.B., Chae,J.H., Choi,M., *et al.* (2021) Loss of function mutations in GEMIN5 cause a neurodevelopmental disorder. *Nat. Commun.*, **12**, 2558.
54. Langmead,B., Trapnell,C., Pop,M. and Salzberg,S.L. (2009) Ultrafast and memory-efficient alignment of short DNA sequences to the human genome. *Genome Biol.*, **10**, R25.
55. Love,M.I., Huber,W. and Anders,S. (2014) Moderated estimation of fold change and dispersion for RNA-seq data with DESeq2. *Genome Biol.*, **15**, 550.
56. Kruger,J. and Rehmsmeier,M. (2006) RNAhybrid: microRNA target prediction easy, fast and flexible. *Nucleic Acids Res.*, **34**, W451–W454.
57. John,B., Enright,A.J., Aravin,A., Tuschl,T., Sander,C. and Marks,D.S. (2004) Human MicroRNA targets. *PLoS Biol.*, **2**, e363.
58. Agarwal,V., Bell,G.W., Nam,J.W. and Bartel,D.P. (2015) Predicting effective microRNA target sites in mammalian mRNAs. *Elife*, **4**, e05005.
59. Uemura,A., Oku,M., Mori,K. and Yoshida,H. (2009) Unconventional splicing of XBP1 mRNA occurs in the cytoplasm during the mammalian unfolded protein response. *J. Cell Sci.*, **122**, 2877–2886.
60. Daigle,J.G., Lanson,N.A. Jr, Smith,R.B., Casci,I., Maltare,A., Monaghan,J., Nichols,C.D., Kryndushkin,D., Shewmaker,F. and Pandey,U.B. (2013) RNA-binding ability of FUS regulates neurodegeneration, cytoplasmic mislocalization and incorporation into stress granules associated with FUS carrying ALS-linked mutations. *Hum. Mol. Genet.*, **22**, 1193–1205.
61. Ragagnin,A.M.G., Shadfar,S., Vidal,M., Jamali,M.S. and Atkin,J.D. (2019) Motor neuron susceptibility in ALS/FTD. *Front Neurosci*, **13**, 532.
62. Sama,R.R., Ward,C.L., Kaushansky,L.J., Lemay,N., Ishigaki,S., Urano,F. and Bosco,D.A. (2013) FUS/TLS assembles into stress granules and is a prosurvival factor during hyperosmolar stress. *J. Cell. Physiol.*, **228**, 2222–2231.
63. Kamelgarn,M., Chen,J., Kuang,L., Jin,H., Kasarskis,E.J. and Zhu,H. (2018) ALS mutations of FUS suppress protein translation and disrupt the regulation of nonsense-mediated decay. *Proc. Natl Acad. Sci. USA*, **115**, E11904–E11913.
64. Birsa,N., Ule,A.M., Garone,M.G., Tsang,B., Mattedi,F., Chong,P.A., Humphrey,J., Jarvis,S., Pisiren,M., Wilkins,O.G., *et al.* (2021) FUS-ALS mutants alter FMRP phase separation equilibrium and impair protein translation. *Sci. Adv.*, **7**, eabf8660.
65. Lopez-Erauskin,J., Tadokoro,T., Baughn,M.W., Myers,B., McAlonis-Downes,M., Chillon-Marinas,C., Asiaban,J.N., Artates,J., Bui,A.T., Vetto,A.P., *et al.* (2020) ALS/FTD-linked mutation inFUS suppresses intra-axonal protein synthesis and drives disease without nuclear loss-of-function of FUS. *Neuron*, **106**, 354.

66. Scekic-Zahirovic,J., Sendscheid,O., El Oussini,H., Jambeau,M., Sun,Y., Mersmann,S., Wagner,M., Dieterle,S., Sinniger,J., Dirrig-Grosch,S., *et al.* (2016) Toxic gain of function from mutant FUS protein is crucial to trigger cell autonomous motor neuron loss. *EMBO J.*, **35**, 1077–1097.
67. Morlando,M., Ballarino,M., Gromak,N., Pagano,F., Bozzoni,I. and Proudfoot,N.J. (2008) Primary microRNA transcripts are processed co-transcriptionally. *Nat. Struct. Mol. Biol.*, **15**, 902–909.
68. Fletcher,C.E., Godfrey,J.D., Shibakawa,A., Bushell,M. and Bevan,C.L. (2017) A novel role for GSK3beta as a modulator of Drosha microprocessor activity and MicroRNA biogenesis. *Nucleic Acids Res.*, **45**, 2809–2828.
69. Rizzuti,M., Filosa,G., Melzi,V., Calandriello,L., Dioni,L., Bollati,V., Bresolin,N., Comi,G.P., Barabino,S., Nizzardo,M., *et al.* (2018) MicroRNA expression analysis identifies a subset of downregulated miRNAs in ALS motor neuron progenitors. *Sci. Rep.*, **8**, 10105.
70. Gascon,E. and Gao,F.B. (2012) Cause or effect: misregulationof microRNA pathways in neurodegeneration. *Front Neurosci*, **6**, 48.
71. Kawaguchi,T., Rollins,M.G., Moinpour,M., Morera,A.A., Ebmeier,C.C., Old,W.M. and Schwartz,J.C. (2020) Changes to the TDP-43 and FUS interactomes induced by DNA damage. *J. Proteome Res.*, **19**, 360–370.
72. Sharma,A., Lyashchenko,A.K., Lu,L., Nasrabady,S.E., Elmaleh,M., Mendelsohn,M., Nemes,A., Tapia,J.C., Mentis,G.Z. and Shneider,N.A. (2016) ALS-associated mutant FUS induces selective motor neuron degeneration through toxic gain of function. *Nat. Commun.*, **7**, 10465.
73. Zou,Z.Y., Liu,M.S., Li,X.G. and Cui,L.Y. (2015) Mutations in SOD1 and FUS caused juvenile-onset sporadic amyotrophic lateral sclerosis with aggressive progression. *Ann. Transl. Med.*, **3**, 221.
74. Grassano,M., Brodini,G., De Marco,G., Casale,F., Fuda,G., Salamone,P., Brunetti,M., Sbaiz,L., Gallone,S., Cugnasco,P., *et al.* (2022) Phenotype analysis of fused insarcoma mutations in amyotrophic lateral sclerosis. *Neurol Genet*, **8**, e200011.
75. Kim,Y.K., Kim,B. and Kim,V.N. (2016) Re-evaluation of the roles of DROSHA, Export in 5, and DICER in microRNA biogenesis. *Proc. Natl Acad. Sci. USA*, **113**, E1881–E1889.
76. Tang,X., Zhang,Y., Tucker,L. and Ramratnam,B. (2010) Phosphorylation of the RNase III enzyme Drosha at Serine300 or Serine302 is required for its nuclear localization. *Nucleic Acids Res.*, **38**, 6610–6619.
77. Link,S., Grund,S.E. and Diederichs,S. (2016) Alternative splicing affects the subcellular localization of Drosha. *Nucleic Acids Res.*, **44**, 5330–5343.
78. Liang,X.H. and Crooke,S.T. (2011) Depletion of key protein components of the RISC pathway impairs pre-ribosomal RNA processing. *Nucleic Acids Res.*, **39**, 4875–4889.
79. Knuckles,P., Vogt,M.A., Lugert,S., Milo,M., Chong,M.M., Hautbergue,G.M., Wilson,S.A., Littman,D.R. and Taylor,V. (2012) Drosha regulates neurogenesis by controlling neurogenin 2 expression independent of microRNAs. *Nat. Neurosci.*, **15**, 962–969.
80. Rolando,C., Erni,A., Grison,A., Beattie,R., Engler,A., Gokhale,P.J., Milo,M., Wegleiter,T., Jessberger,S. and Taylor,V. (2016) Multipotency of adult hippocampal NSCs in vivo is restricted by Drosha/NFIB. *Cell Stem Cell*, **19**, 653–662.
81. Beezhold,K.J., Castranova,V. and Chen,F. (2010) Microprocessor of microRNAs: regulation and potential for therapeutic intervention. *Mol. Cancer*, **9**, 134.
82. Yang,Q., Li,W., She,H., Dou,J., Duong,D.M., Du,Y., Yang,S.H., Seyfried,N.T., Fu,H., Gao,G., *et al.* (2015) Stress induces p38 MAPK-mediated phosphorylation and inhibition of Drosha-dependent cell survival. *Mol. Cell*, **57**, 721–734.
83. Eitan,C. and Hornstein,E. (2016) Vulnerability of microRNA biogenesis in FTD-ALS. *Brain Res.*, **1647**, 105–111.
84. Kmetzsch,V., Latouche,M., Saracino,D., Rinaldi,D., Camuzat,A., Gareau,T., French Research Network on,F.A., Le Ber,I., Colliot,O. and Becker,E. (2022) MicroRNA signatures in genetic frontotemporal dementia and amyotrophic lateral sclerosis. *Ann Clin Transl Neurol*, **9**, 1778–1791.
85. Shioya,M., Obayashi,S., Tabunoki,H., Arima,K., Saito,Y., Ishida,T. and Satoh,J. (2010) Aberrant microRNA expression in the brains of neurodegenerative diseases: miR-29a decreased in Alzheimer disease brains targets neurone navigator 3. *Neuropathol. Appl. Neurobiol.*, **36**, 320–330.
86. Luo,H.C., Yi,T.Z., Huang,F.G., Wei,Y., Luo,X.P. and Luo,Q.S. (2020) Role of long noncoding RNA MEG3/miR-378/GRB2 axis in neuronal autophagy and neurological functional impairment in ischemic stroke. *J. Biol. Chem.*, **295**, 14125–14139.

Received: January 19, 2023. **Revised:** August 3, 2023. **Editorial Decision:** August 25, 2023. **Accepted:** September 12, 2023